The University of Manchester Research

Dynamics and stratigraphy of a tidal sand ridge in the Bristol Channel (Nash Sands banner bank) from repeated high-resolution multibeam echo-sounder surveys

DOI:
10.1111/sed.12935

Document Version
Accepted author manuscript

Link to publication record in Manchester Research Explorer

Citation for published version (APA):
Mitchell, N., Jerrett, R., & Langman, R. (2021). Dynamics and stratigraphy of a tidal sand ridge in the Bristol Channel (Nash Sands banner bank) from repeated high-resolution multibeam echo-sounder surveys: Sand ridge dynamics from repeated sonar surveys. *Sedimentology*. https://doi.org/10.1111/sed.12935

Published in:
Sedimentology

Citing this paper
Please note that where the full-text provided on Manchester Research Explorer is the Author Accepted Manuscript or Proof version this may differ from the final Published version. If citing, it is advised that you check and use the publisher's definitive version.

General rights
Copyright and moral rights for the publications made accessible in the Research Explorer are retained by the authors and/or other copyright owners and it is a condition of accessing publications that users recognise and abide by the legal requirements associated with these rights.

Takedown policy
If you believe that this document breaches copyright please refer to the University of Manchester's Takedown Procedures [http://man.ac.uk/04Y6Bo] or contact uml.scholarlycommunications@manchester.ac.uk providing relevant details, so we can investigate your claim.

Download date:12. Nov. 2022

Dynamics and stratigraphy of a tidal sand ridge in the Bristol Channel (Nash Sands banner bank) from repeated high-resolution multibeam echo-sounder surveys

Running title: Sand ridge dynamics from repeated sonar surveys

Neil C. Mitchell[1*], Rhodri Jerrett[1], Rob Langman[2]

[1]Department of Earth and Environmental Sciences
University of Manchester
Williamson Building
Oxford Road
Manchester M13 9PL, U.K.

[2]Marinespace Ltd.
Ocean Village Innovation Centre
Ocean Way
Southampton
Hampshire SO14 3JZ, U.K.

This is the green open-access version of the above-titled article accepted for publication on 16 August 2021 with the Wiley journal "Sedimentology".

Abstract:

Repeated multibeam echo-sounder surveys can provide information on developing stratigraphy over large areas and during periods when environmental conditions are known. Here, we use 13 time-separated multibeam echo-sounder surveys between 2002 and 2010 of a tidal sand ridge in a macrotidal estuary: Nash Sands, a banner bank in the Bristol Channel (U.K.). Over the surveyed period, Nash Sands was S-shaped in plan-view, with two *en échelon* segments separated by a channel (swatchway). Migration of these inflections along the ridge led to deposition of clinoforms up to 5°-7° steep and 12-14 m tall. The clinoforms downlapped onto their substrates or onto cross-sets formed by dunes migrating clockwise around the lower flanks of the ridge. Clinoform topsets were removed or truncated by repeated erosion and/or dune migrations over the ridge crest and replaced with packages of near-horizontal laterally discontinuous irregular beds. Flank dune crests were oriented obliquely to nearly perpendicularly to the clinoforms in all three sets, so the clinoforms developed by oblique-lateral accretion locally. Although one area had strongly eroded in the prior decade during elevated wave conditions, the 2002-2010 stratigraphic development revealed a different relationship with extreme wave heights; Nash Sands generally accumulated sand during times of more extreme waves and lost sand during more quiescent conditions. Using also single-beam survey data from 1991-2002 to study the ridge morphology over 19 years to 2010, the swatchway was absent in 1991-1992 and progressively developed as the ridge sinuosity became more accentuated. Dunes found migrating NW through the swatchway are potential

evidence of a current caused by tidal height differences across the ridge during ebb conditions. The study illustrates how repeated sonar measurements reveal the processes and timescales that lead to the deposition of stratigraphic units.

Keywords: clinoforms, tidal banner bank, headland-attached bank, tidal sand ridge, multibeam sonar, marine sand dunes, Bristol Channel

Introduction

In the stratigraphic literature, tidal sand ridges are linear features predominantly found on continental shelves, with long axes oriented subparallel to the prevailing tidal current ellipse (Reynaud and Dalrymple, 2012). They have been referred to as "sand banks" in the oceanographic literature and can reach 200 km in length, 15 km in width and 55 m in height (Belderson et al., 1982; Stride et al., 1982). Tidal bars are comparable features lying within tidal channels (Dalrymple, 2010). Numerical models show how sand is typically transported parallel to the crests of shelf tidal ridges but turns (veers) progressively into shallower water, thus transporting sand towards their crests, causing them to grow until wave activity and tidal current friction limit their heights near sea level (Huthnance, 1982a; Huthnance, 1982b; Harris, 1988; Hulscher et al., 1993; Reynaud and Dalrymple, 2012). The ridge-parallel transport is revealed by the presence of transverse bedforms (dunes), which migrate and have asymmetries suggesting a circulation of the sand around the ridges (Belderson et al., 1982). However, more complex non-equilibrium behaviour is typically suggested by historical bathymetric data (Caston, 1972) and stratigraphy from seismic surveys (Berné et al., 1994; Berné et al., 1998).

Modern tidal ridges are sources of commercial aggregates, form substrates for offshore infrastructure such as windfarms and present hazards to shipping. Consequently, there is a practical need for enhanced understanding of tidal ridges, including how and how rapidly they change morphology over time, their rates of migration across shelves, and how and when they become moribund. Also relevant to coastal management, there have been two competing models for sand transport in the Bristol Channel. Stride and Belderson (1990) envisaged the stronger ebb currents observed along the axis of the Bristol Channel to dominate sand transport, except for local circulation around tidal sand ridges. In contrast, others (Collins and Ferentinos, 1984; Harris and Collins, 1991) have interpreted the results of tidal models, float movements and geophysical data as indicating that some sand transport occurs up-estuary near to the coasts driven by flood-dominating currents. This type of issue can be difficult to resolve by modelling, but sand dune movements can be used to evaluate dune-associated bedload fluxes (Schmitt and Mitchell, 2014), so the results here illustrate the potential benefits of time-lapse surveying for coastal management.

In the rock record, tidal ridge or bar deposits can be difficult to identify, though a number have been proposed (Tillman and Martinsen, 1984; Gaynor and Swift, 1988; Mellere and Steel, 1995; Martinsen et al., 1999; Yoshida, 2000; Plink-Björklund and Steel, 2006; Plink-Björklund, 2008; Steel et al., 2008; Pontén and Plink-Björklund, 2009; Hampson, 2010; Michaud, 2011; Martinius, 2012; Olariu, M. et al., 2012; Scasso et al., 2012; Steel et al., 2012; Chen et al., 2014; López et al., 2016; Michaud and Dalrymple, 2016; Sharafi et al., 2016; Longhitano et al., 2021). In particular, there has been some debate concerning how tidal ridges can be discriminated from other tidally-influenced deposits. The style of accretion has been proposed to be a useful discriminator, with tidal ridges expected to accrete laterally or obliquely to residual currents, whereas dune complexes are expected to involve forward accretion (Olariu, C. et al., 2012). However, while lateral accretion has been commonly shown to occur in linear tidal ridges on open continental shelves (clinoforms in seismic data demonstrate how ridges have migrated perpendicular to currents (e.g., Berné et al., 1994)), it has been less clear if lateral accretion would be found in more complex ridges or in ridges attached to headlands such as Nash Sands, which have less scope to migrate laterally. The understanding developed from time-lapse multibeam sonar results, such as those presented here, can potentially help researchers recognise tidal ridges when preserved in outcrop. In our view, geological interpretation of outcrops more generally could be better informed by such time-lapse geophysical datasets from modern environments.

Nash Sands, a tidal sand ridge in the Bristol Channel (Figure 1), was surveyed biannually for a consortium of aggregates companies from 2003 until 2010, following a decade of single-beam echo sounder monitoring (Lewis et al., 2015). This dataset comprises 12 complete multibeam surveys of the ridge and adjacent seabed areas. For context, each multibeam dataset involved ~500-600 line-km of surveying. At a modest 5 knots needed for inshore work, each survey would have taken 54-65 hours, or likely two weeks considering transit times to/from port and times required for sound velocity measurements and installations/retrievals of tide gauges when used. With also occasional weather and equipment outages, each survey typically took three weeks to carry out. A multibeam survey in the summer of 2002 collected a further dataset of easterly Nash Sands (Schmitt, 2006). The full dataset extends 15 km east-west by 6 km north-south (Figure 2) and is represented by data grids with cell sizes of 1-2 m.

Broader significance of time-lapse surveying to sedimentology

Tremendous advances have been made in characterizing stratigraphic geometries in 3D down to a few m vertical resolution, thanks to the development of the 3D seismic reflection method and its widespread use by the oil and gas industry (Posamentier and Kolla, 2003). In contrast, for information needed to understand bed development at <1 m vertical resolution, most work has only been possible in 1D (boreholes), 2D (outcrops) or at best in a coarse form of 3D only by interpolation between boreholes or outcrops. Stratigraphy can be resolved in 3D or near 3D with boomer grid surveys (Berné et al., 1993; Marsset et al., 1999) and 3D Chirp at c. 10 cm scale (Bull et al., 2005), but the stratigraphy from these systems is typically compromised by incompleteness or poor penetration in sands in the case of Chirp. However, a more important restriction to understanding how stratigraphy develops is typically poor knowledge of the chronology of deposition and the environmental conditions accompanying deposition. In contrast, monitoring with benthic landers containing current meters, altimeters, cameras, nephelometers, etc. can provide rich data time-series on re-suspension and deposition (e.g., Tengberg et al., 1995), but the information is very localized.

Time-lapse surveying with multibeam and other sonars (Tengberg et al., 1995; Knaapen et al., 2005; Kostaschuk and Best, 2005; Mitchell, 2005; Wienberg and Hebbelm, 2005; Ernsten et al., 2006; Schmitt, 2006; Buijsman and Ridderinkhof, 2008; Schmitt et al., 2008; Xu et al., 2008; Bosman et al., 2014; Schmitt and Mitchell, 2014; Kelner et al., 2016; Bosman et al., 2020; Guiastrennec-Faugasa et al., 2020) now offers the possibility of providing stratigraphic information in 3D and over large areas for which the history of deposition is well known from the survey dates. Successively measured seabed surfaces effectively represent stratal boundaries if preserved. Reconstruction of stratigraphic surfaces in this manner has led to important improvements in our understanding of sediment transport, deposition and remobilisation in marine settings. For example, time-lapse multibeam surveys in western Canadian fjords have revealed that sediment gravity flows there often occur without clearly identifiable triggers and steep prodelta channels can be dominated by the upstream migrations of antidunes or 5-to-30-m-high cyclic steps produced by those flows (Talling et al., 2015; Hughes Clarke, 2016; Hage et al., 2018; Hizzett et al., 2018; Vendettuoli et al., 2019; Heijnen et al., 2020).

Background to Nash Sands and its environment

The sediments within the Bristol Channel were deposited during or shortly after the last glaciation, with very little supplied by modern rivers (Hamilton et al., 1979). During the Flandrian transgression (3-5 ka BP), sea level reached its present level in the Bristol Channel (Jennings et al., 1998) and the modern tidal regime became established (Stride and Belderson, 1990). Gibbard et al. (2017) showed outer end moraine underlying westerly Nash Sands, which correspond with the undulating morphology marked "glacial till" in Figure 2. At its easterly end, the ridge is underlain by Jurassic strata, which outcrop below Nash Point (Lloyd et al., 1973; Evans and Thompson, 1979; Bourne and Willemse, 2001). A series of ridges of 2-3 m relief are observed south of East Nash, with sharp truncations in places (Figure 2). These correspond to sampled Lias strata (Lloyd et al., 1973; Evans and Thompson, 1979), so the ridges are likely the result of differential erosion of Lias beds. Some further ridges, though of lower relief and less distinct, can also be observed in the multibeam data immediately north of East Nash.

Nash Sands is a banner bank, a type of tidal sand ridge that emanates from a headland, in this case Nash Point (Figure 1). Such banner banks, also called “headland associated banks” (Berthot and Pattriaratchi, 2006b), are thought to develop as a result of differing flood and ebb currents, which lead to eddies in the residual (tidally averaged) current adjacent to headlands, with sand accumulating within those eddies (Pingree, 1978; Ferentinos and Collins, 1980; Dyer and Huntley, 1999; Yin et al., 2003; Berthot and Pattriaratchi, 2006b; Neill, 2008; Neill and Scourse, 2009). Hence, Lewis et al. (2015) refer to Nash Sands as a "residual tidal circulation induced bank". Alternatively, such ridges may develop by convergence of sand transported in transient eddies (Signell and Harris, 2000; Bastos et al., 2002; Li et al., 2014). Heathershaw and Hammond (1980) have also suggested that helical secondary circulations like those produced at meander bends in rivers could also play a role in their development. Once developed, the morphologies of the ridges themselves modify the currents and sand transport, modulating the subsequent evolution of the ridges (Berthot and Pattriaratchi, 2005; Berthot and Pattriaratchi, 2006b).

Sedimentary bedforms and sand transport have been studied extensively in the Bristol Channel (Ferentinos, 1978; Ferentinos and Collins, 1980; Pattiaratchi and Collins, 1984; Harris and Collins, 1985; Collins, 1987; Harris and Collins, 1988; Stride and Belderson, 1990; Harris and Collins, 1991; Stride and Belderson, 1991). Shallow seismic reflection data have been reported as showing that Nash Sands has grown on an essentially flat bedrock substrate (Ferentinos and Collins, 1980). Sand transport around Nash Sands is dominated by eastward flood currents on its north side and by westward ebb currents on its south side, hence dunes generally circulate clockwise around it (Ferentinos and Collins, 1979; Collins and Ferentinos, 1984; Harris and Collins, 1985; Collins, 1987; Harris, 1988; McLaren et al., 1993; Schmitt, 2006). From echo-soundings collected with a 263-day separation, Schmitt (2006) found that dunes on the SE flank of Nash Sands were migrating at 139-179 m y^{-1} annualised rates in the ebb current (westerly) direction. Fairley et al. (2016) developed a numerical model to investigate how storms and surges could affect the ridge. Their model suggests that the southerly side of easterly Nash Sands could be an area of deposition if storm and surge conditions coincide with spring tides. Also highlighting the importance of storms, Lewis et al. (2015) found links between the cross-sectional shape of Nash Sands and measures of storminess for the decade prior to 2000.

Tidal currents are enhanced within the central Bristol Channel by the funnelling effect of the estuary (Owen, 1980; Uncles, 1983). A numerical tidal model of Ahmadian et al. (2014) shows a maximum spring tidal current of 2.0 m s^{-1} just south of Nash Point, declining by almost a factor of two towards the westerly end of Nash Sands. The model of Fairley et al. (2016) predicted that currents could exceed 2.0 m s^{-1} along the whole of Nash Sands if a storm surge coincides with a spring tide. Figure 3a shows current meter data collected by Harris and Collins (1988) immediately south of Nash Point (site CM2 in Figure 2). Based on the data from that current meter and sand physical properties, they estimated that sand flux locally was 57.7 tonne cm^{-1} yr^{-1} towards 307° (currents exceed 100 cm s^{-1} more often to the WNW (ebb current) than they do to the ESE (flood current)). Tidal range also recorded at CM2 was 4.5 and 8.6 m during neap and spring tides, respectively. Sediment recovered by grab sampling on Nash Sands typically has a 0.3 mm grain size, i.e., medium sand (Figure 2). Based on a grain size of 0.3 mm and current meter data from site CM2, Schmitt (2006) predicted that the bed shear stress would be almost continuously above the sand threshold of motion during both spring and neap tides except for very brief periods during slack water.

To assess wave conditions over the decade of the surveys, we obtained outputs from the ERA global analysis of wind speeds and other meteorological data (Caires and Sterl, 2003; Dee et al., 2011) (https://www.ecmwf.int/). (ERA represents ECMWF ReAnalysis, where ECMWF is the European Centre for Medium-Range Weather Forecasts.) Mitchell et al. (2012b) have shown that these data can be accurate where waves are not blocked by small offshore islands and associated bathymetry that are missing from the ERA model. To extract wave data from the ERA model, we therefore chose a site within the centre of the channel (Figure 1) where waves from predominantly westerly winds should be well represented. The heights of those waves were sorted into quarter-year intervals, from which cumulative distributions were derived. Figure 3b shows various percentiles of those distributions, with those above 90% shown every additional

1% to highlight the more extreme conditions. For considering possible storm surge occurrences, we also show the water level elevation extremes in Figure 3c for a tide gauge at the Mumbles located in Figure 1. Higher extremes indicate times when tidal currents were likely enhanced by storm surge (Fairley et al., 2016) and hence when we might expect greater changes in Nash Sands.

During the 2002 multibeam survey and during visits to the adjacent coastline in 2003, waves were observed breaking along the front of Nash Sands during low tide. Sand was dredged from the periphery of West Nash for local construction purposes, which according to HR Wallingford Ltd. (2016) averaged 7.2 X 10^8 kg y^{-1}. Some pits observed in the multibeam bathymetry over West Nash may be due to dredging ("Extraction pits" in Figure 2).

Acquisition of datasets and processing

The multibeam data were collected from 2003 onwards by the survey companies Andrews, Lamkelma-Andrews and Gardline Environmental under contract to the consortium of aggregates companies (Hanson Aggregates Marine, Tarmac Marine Dredging and CEMEX UK Marine). Each survey typically covered Nash Sands completely, along with subtidal parts of the adjacent coast of Wales and the sea area between the Welsh coast and Nash Sands (Figure 2). The total area covered in August 2008, for example, was 57 km^2.

Details of these surveys are incomplete (Table 1), though company reports reveal that bathymetry data were collected with a Geoacoustics Geoswath system along with a TSS DMS-05 motion sensor. Positioning was by differential GPS (DGPS), followed by combined DGPS and kinematic GPS (KGPS) from August 2008 onwards. The KGPS system collected accurate vessel height data, which were used for tidal height corrections of the soundings. As tidal height and phase vary around the Bristol Channel, these tidal corrections should be the most accurate across the surveyed area. Before August 2008, data from portable tide gauges (Valeport Midas Water Level Recorders) were used to correct for tides, though in 2003 and February 2004, data from the Port Talbot tide gauge were used. The Port Talbot gauge was also used in March 2008 due to unplanned movements of the deployed portable gauges. Vertical differences between the February 2004 dataset and adjacent years of a few metres occurring in bands aligned with the survey vessel tracks (Figure 4) suggest the presence of local tidal height errors. Otherwise the datasets appear to have been tide-corrected well. The 2002 multibeam data were collected with a 101-beam Reson Seabat 8101 240 kHz sonar (Schmitt, 2006) and processed as described previously (Schmitt et al., 2008; Schmitt and Mitchell, 2014). All depth data presented here are referenced to Chart Datum, hence zero depth in the figures corresponds with lowest astronomical tide.

The data have varied quality and resolution, arising from varied weather conditions, survey practices and equipment. The 2002 dataset was gridded with a 1 m cell size, as seabed feature position mis-matches at overlapping swaths suggest the DGPS precision was ~1 m or less (Schmitt, 2006). A study of vertical uncertainties in parts of those data over bedrock adjacent to Nash Sands by Schmitt (2006) using the method of Schmitt et al. (2008) found 2-standard deviations of measured depth variations of only ~0.25 m. The other datasets were supplied as grids with 2 m cell size, apart from the 2003 dataset, which was only available to us with a 4-m cell size. The data appear to be degraded to varying extents by motion sensor and other noise, likely related to varied weather conditions, also affecting the resolution of seabed topography in practice. Figure 2 shows a map from the August 2008 survey derived from some of the highest quality data. Time-lapse sequences of the whole dataset and enlargements in map view are shown in the electronic supplement (Figures A1a-A1d). We recommend that readers view these sequences to get the best overall impression of the dataset.

Method

Profiles were formed along the lines marked in Figure 2 in order to cross the depositing areas marked in Figure 5 and sampled from each of the multibeam survey datasets. The profiles in Figure 6 are essentially parallel to the general direction of residual (tidally-averaged) currents along the south side of Nash Sands during spring tides according to the models of Fairley et al. (2016), whereas the profiles in Figure 7 are perpendicular to that direction. Hence, the former profiles are approximately parallel, and the latter approximately perpendicular to, the directions of sediment transport predicted by tidal models.

For each longitudinal profile, we identified segments that are unlikely to have received or lost much sand between surveys, because they comprise bedrock ridges or in one case a hill in the glacial till. These segments highlighted in black along each profile in Figure 2 were used as benchmarks to assess bias between survey lines. We computed a mean elevation for each survey along these segments. Using the mean of those averages for each benchmark, we computed a deviation for each survey. For the six profiles and 12 surveys (2003-2010), the 72 deviations had a root-mean-square (RMS) value of 0.21 m. As this contains some uncertainty due to bottom detection, motion sensor, sound velocity and other measurement errors (Schmitt et al., 2008), the biases due to tidal height errors should be much less than 0.21 m on average. (For example, some oscillations of the surface immediately north of "N2" in Figure 2 are likely due to inaccurate recording of vessel motion by motion sensors.)

For each profile located in Figure 2, we adjusted the elevations to the August 2008 survey data (a higher-quality dataset) using offsets over the benchmarks. Successive survey elevations were checked to see if they lay below elevations of preceding surveys, implying that erosion of those earlier seabed surfaces had occurred. Removing those "eroded" surfaces of prior surveys, we built time-lapse sequences that illustrate the build-up of the stratigraphy. This procedure is similar to that used in the numerical modelling of stratigraphy by Rubin (1987). These sequences are provided in the electronic supplement to this article (Figures A2-A8).

To provide the pseudo-stratigraphic profiles across the ridge, we repeated this procedure for the blue lines located in Figure 2 though without adjustments for tidal height errors affecting individual swaths, which were not easy to implement with the grids provided to us. However, as the above RMS variations found above were only 0.21 m (a small value considering that some elevation changes reached ~10 m (Figure 6)), we suspect these sections will not be significantly affected by tidal errors, except locally such as for the February 2004 error mentioned earlier. The results are shown in Figure 7.

We also repeated this exercise on the multibeam bathymetry data in map view, also without adjustments for tidal height error. Maps are shown of deposit thicknesses (Figure 8) and horizon topography (Figure 9), where surfaces had not been eroded by February 2010. In Figure 10, we show an estimate of the stratigraphic completeness, which is the ratio of net deposition over the interval (February 2003 to February 2010) divided by the sum of all deposit thicknesses over that interval. As discussed by Vendettuoli et al. (2019), this measure is over-estimated as it is not possible to capture all the intervals of deposition with intermittent surveys, but it nevertheless reveals broad areas where the stratigraphy would have been better preserved over the duration of the surveys.

Observations

Morphology and evolution of the ridge

The multibeam sonar surveys (Figures 2 and A1) reveal Nash Sands as having a more complicated structure than a simple straight ridge. It is weakly sinuous in plan-view. Its eastern half ("East Nash") emerges at extreme spring tides and has shallow linear bedforms oriented WSW-ENE overlying its flat top. The flat top most likely results from surface waves and tidal current friction limiting the upward growth of the ridge (Huthnance, 1982a). In contrast, the westerly half ("West Nash") has a crest that is sharper and several metres deeper. The westerly third of West Nash is also superimposed with WSW-ENE bedforms (dunes). Elsewhere dune crestlines are more nearly north-south oriented, though with curved terminations and with SW-NE crests connecting flank dunes over the crest of West Nash, as observed at the crest of nearby Helwick Sands (Schmitt et al., 2007; Schmitt and Mitchell, 2014). Between the shallow summits of West and East Nash is a deeper area almost forming a channel crossing the ridge, though blocked by a sharp-crested ridge on the north side. Although this depression does not extend across the whole of Nash Sands, crossing channels somewhat similar to it have elsewhere been called swatchways (Cloet, 1954; Robinson, 1960; Dalrymple and Rhodes, 1995), so we adopt this term here to aid discussion.

The cross-section of the ridge is asymmetric, with steeper southerly flanks on both halves, though with a steeper northern half at the swatchway. Dune asymmetry and the migrations of dunes revealed in the animation (Figure A1a) suggest general clockwise movement of sand around the ridge, as predicted by tidal models (Fairley et al., 2016). Those models were generated with bathymetry data that had lower resolution and different ridge height than is presented here and they predicted that residual currents cross the ridge from NW to SE, as would be expected conceptually from the funnel effect of the ridge and coast on the flood tide. In contrast, the multibeam data animation (Figure A1a) reveals dunes migrating to the NW in the swatchway. In the NW part of the swatchway, two sets of overlapping dunes with differing orientations migrated towards the NNW and NW. Their migrations are revealed in cross-section x-x' (Figure 11).

Between 2003 and 2010, five areas accumulated sediment (Figure 5), in the case of area D1 by more than 13 m. Four areas were eroded, though with generally lesser elevation changes. These accumulations and erosions were also associated with a change in plan-view shape of the ridge (Figure A1a). The ridge crestline at D3 located in Figure 5 moved west-northwest, while the promontory at D1 became more pronounced and angular, while also moving west-northwest. Figure 12a shows that the magnitudes of cumulative volumes for the north flank areas were roughly equal, whereas those in the south flank were more irregular, with D1 accreting more than double the sediment volume of the other areas. The south flank polygons accumulated a net 3.42 X 10^6 m^3, while the north flank polygons lost 0.5 X 10^6 m^3.

Further detail is provided by the time-series in Figure 12b calculated from the changes in sediment volumes divided by differences in the central date for each survey. These rates are affected by the uncertainties in tidal height errors and because some survey dates are poorly known, hence data before 2005 are excluded. For surveys before late 2007, we only know an indicative month for each survey. For the later surveys, where tidal height was better constrained with kinematic GPS, uncertainty in the dates still affects these rates as we do not know exactly when during each survey period each polygon was surveyed. In Figure 12b, we provide uncertainty bars to represent the extreme effects of date uncertainty. Maximum rates assume each polygon was surveyed in the last day of a survey and then on the first day of the subsequent survey. Similarly, minimum rates assume they were surveyed on the first and last days of each pair of surveys. However, the surveys were more likely carried out systematically with similar track plans, so these uncertainties are likely exaggerated. Considering that the uncertainties in Figure 12b scale with annualised volume change (as date uncertainty affects the divisor), the differences between curves are generally resolved from late 2007 onwards.

From Figure 12b, the stratigraphy within D1 developed at a steadily increasing rate, though briefly with a smaller rate in late 2008 and in the summer of 2009, coinciding with a period of lower wave heights and somewhat lower extreme water levels (Figure 3). Deposition in D2 and D3 also was slow in late 2008 and in the summer of 2009. However, erosion rates in other areas (E1-E4) were high over this period.

There appear to be synchronous variations within two groups. West Nash E2, D2 and E3 all peaked in late 2007, whereas East Nash D3, E4, D4, D5 and E1 all peaked in early 2008. In late 2009, all areas except E1, D3 and D5 experienced a positive acceleration in volume (either greater deposition or less erosion).

Stratigraphy

Although seabed surfaces do not necessarily lead to stratigraphic surfaces, the results of the numerical results presented here hint at how stratigraphy develops. In practice, truncation of multibeam surfaces by later surfaces may under-represent the intervening erosion if the bed was lower between successive surveys. In the 1-m-resolution 2002 data, megaripples are observed (Figure 13) (Schmitt and Mitchell, 2016). Dalrymple (1984) showed how migrations of megaripples generate much of the fine-scale stratigraphy within dunes, including herringbone structures by migration during the subordinate tide. Those, and intermittent erosion occurring during the subordinate tide, can lead to complex stratigraphic structures produced by the larger bedforms that otherwise appear to be translating simply. The pseudo-stratigraphic sections presented here therefore need to be interpreted as evidence of net accumulation within which more complex stratigraphic structures may have developed.

We first investigate how the surfaces appear along the two sets of profiles and hence how they might appear in ridge parallel and perpendicular seismic reflection profiles. However, for comparison with observations of field outcrops, where the overall geometry of a ridge may be less obvious, it is useful to consider the geometries of surfaces in three dimensions (3D), as both sets of sections in Figures 6 and 7 were drawn obliquely to the local dips of the bathymetry. Hence, we later address geometries in 3D.

Ridge-parallel profiles

Ridge-parallel profiles S3 and S1 (Figures 6a and 6b) reflect accretion on lee slopes lying approximately down expected residual current directions. Profile S3 (Figure 6a) illustrates deposition in area D1 apparently of a succession of surfaces that were inclined down-current up to 10 m high. Gradients were typically 1.5°-2.0° along the line of section (in contrast, local gradient maxima dipping SW were 5°-7° in the upper ridge flank). Earlier surfaces had sigmoidal geometries, with well-developed apparent topsets and bottomsets. Their clinoform-like surfaces were smooth, i.e., sand waves were not developed on their surfaces (at the resolution of the survey data). The bottomsets downlapped directly onto the substrate. The topsets were removed by erosion. Consequently, the remaining stratigraphy comprised a succession of top-truncated clinoform-like surfaces, lacking topsets, but potentially with well-developed bottomsets downlapping onto the substrate.

Later surfaces involved dunes in their lower parts. The shapes of the dunes varied strongly, with some forming or reforming between surveys. This makes dunes difficult to track between surveys in this profile, but with the aid of recognizable dune shapes in plan-view (Figure A1b) we were able to associate some of them. In Figure 6a, we connect their troughs. Scour in dune troughs as dunes migrate may be expected to produce bedding surfaces truncating cross-stratification below them. We suggest that this is broadly possible here, although in detail the surfaces may be formed by scour in troughs between superimposed megaripples (Dalrymple, 1984). The trajectories of the dune troughs relative to horizontal suggest that they climbed down-flow with gradients of up to 1.5%. In this area of deposition, the result was potentially a succession of weakly climbing cross beds 1-2 m thick, sitting on the substrate, downlapped by later clinoforms at the scale of the survey data. These later clinoforms had less well developed apparent toesets. The last clinothems had well preserved apparent topsets, but evidence from the earlier clinothems suggests that these topsets did not have much preservation potential.

Profile S1 in area D2 contained a succession of surfaces that dipped down-current, appearing to be forward-accreting along the profile (as we will see later, this is an artefact of the profile orientation). Superimposed on them were westward (down-current) translating dunes. There were many internal erosion surfaces. Association of dunes between surveys reveals that they had modest gradients of climb of <0.5%, with some negative climb gradients. The many internal erosion surfaces were associated with the lower angles of climb compared with the dunes in Profile S3, resulting in a greater degree of truncation of preceding dune surfaces. Mapped surfaces here suggest that a succession of almost flat, tabular cross bedding was produced. The upper parts of the ridge flank do not contain prominent bedforms at the scale of the multibeam data. They formed a succession of shorter (400 m long), discontinuous, down-current accreting clinoform-like surfaces lacking well-developed apparent bottomsets and topsets, which overlay the cross-bedded succession. The lower-flank dunes in the earlier surfaces (at ~2700 m distance in Figure 6b) were less well-developed compared with those in the later surfaces further west, where the lower flank extended to greater depths. There, dunes exceeded 2 m in height. The upper part of this overall structure also had erosional truncations.

Profile N2 in area D3 contained a succession of surfaces that dip in the direction opposite to that of the residual current expected to run west to east on the north side of the ridge, apparently accreting backwards along the section (Figure 6c; as we show later this impression also is an artifact of the section). Surfaces were up to 12 m tall, and had gradients of up to 2° along the profile and 5° local maximum gradients (northwards). Here, dunes formed over the lower and middle of the depositional surfaces. At the crest of Nash Sands, the topsets of the clinoform-like features were truncated. Some truncations affected steeply dipping surfaces and others suggest entrenchments by bedform troughs. With no intervening data available to us, we cannot be sure entrenchments occurred or if bedforms migrated laterally into place, which would have left cross-stratified beds. Between them would have been a number of sub-horizontal discontinuous layers of strongly varied thickness, possibly resembling the Complex Cross-Bedded Cosets found in the crests of sandwaves by Dalrymple (1984).

We simplify the above observations in Figure 14. The stratigraphy appears similar to case V of Allen (1980).

Ridge-perpendicular profiles

The ridge-perpendicular cross-sections C1, C2 and C4-C8 in Figure 7 intersect areas of net deposition D1-D3. Cross-section C3, lying intermediate between D2 and D3, where there was little net accumulation, illustrates the potential effects of dune migrations and erosion over the crest.

C6-C8 over D1 (East Nash) suggest that a near-continuous deposition of thin clinothems occurred. Although the subordinate tide is likely to have caused intermittent erosion, few truncations of surfaces were recorded by the surveying. The result was a succession of apparent clinoforms 10-15 m tall, with gradients of up to 7°. The clinothems had sheet-like geometries with few or no toe-sets. Any topsets that were deposited were largely removed. Bedforms were absent or unresolvable on clinothem surfaces, except towards their lower parts (e.g., C6). Individual clinothems were eroded in places, largely in their lower parts, likely by the passage of dune troughs as they migrated in the direction orthogonal to the cross section. This suggests that a lower succession of cross strata may have been generated, down on to which the later clinoforms downlapped.

Crossing area D3, C4 suggests discontinuous clinothems, whereas C5 suggests sheet-like clinothems similar to those of C6-C8. Both sections show only limited toe-sets. Top-sets of both profiles were eroded, leaving truncated clinoforms.

C1 and C2 from West Nash (D2) contain a different stratigraphy. The inclined seabed surfaces are more irregular and suggest that the formed strata would also have been more irregular, representing deposition from a succession of dunes whose crests were oblique to the line of section. The complexity of the stratigraphy would likely have been even greater than shown in practice due to the effects of the subordinate tide mentioned earlier. Clinothems were also more extensively truncated by the passage of dune troughs between surveys. The stratigraphy generated likely comprised a succession of up to 12 m thick tabular cross-beds. Here the upper part of the succession was also truncated by the passage of dunes over the top of the ridge, which deposited thin, sub-horizontal and discontinuous cross-stratified beds that overlay the dipping cross-stratified strata.

Structures in 3D (the geometry of clinoform accretion)

The apparent deposit thicknesses (Figure 8) were large in spatial extent for D1 through most of the period 2003-2010, with continuous deposition along the upper flank of the ridge and more discontinuous deposition in the lower flank in the area of the dunes. This apparently led to widespread seabed surfaces remaining by 2010 in Figure 9. Mapped intervals between surfaces were more discontinuous in area D2, suggesting that stratigraphy would also have been more complex there than in D1. D3 experienced no deposition until 2004. Deposition occurred for the five years after then, with the greatest thickness deposited in a short period February 2005 to June 2005, although the rates are subject to large survey date uncertainties as mentioned earlier. This intermittent deposition was also reflected in the remaining surfaces in Figure 9, which formed a nearly continuous arc in D3 from February 2005 onwards, occasionally broken by dunes (e.g., August 2008).

To interpret the style of accretion within D1-D3, we define the accretion direction as perpendicular to the general depth contours of the upper flank of the ridge within each of those accreting areas (the upper flanks ultimately formed the clinoform-like surfaces). The direction of the local residual current or dominant formative current within those areas is anticipated to have been perpendicular to the dune crestlines (in studies of rock outcrops, the dip directions of cross-stratification produced by migrating dunes would instead be used, but they would be nearly perpendicular to the original dune crests). Hence, a laterally accreting deposit would have dune crestlines oriented perpendicular to the bathymetric slope of the larger accreting deposit and an obliquely accreting deposit would have crestlines nearer to 45° to the bathymetric slope. A forward-accreting deposit would have dunes migrating in a similar direction to the accretion direction (we suggest dune crestlines within 45° of the slope strike direction as a criterion). In assessing the accretion geometry, the enlarged time-lapse maps in Figures A1b-Ad are useful for revealing how the directions of dune migrations relate to the flank accretion direction. Figure 15 summarises as directional histograms the orientations of dune crestlines in the whole multibeam time-series relative to the flank strike directions of each of the accreting deposits.

Within deposit D1, the dunes at the base of the slope (Figure 2) had crestlines lying at high angles to the strike of the slope. In Figure 9, the dune surfaces remaining by February 2010 formed fingers striking at varied angles from the WNW-ESE strike of the SSW-facing slope. For example, in the March 2009 panel, they lay at $\sim 50^\circ$ to the slope. This obliquity occurred from August 2008 onwards, whereas some dunes were more nearly perpendicular to the SSW-facing surface from September 2003 to June 2006. The dune crest orientations summarized in Figure 15 span a range of $>90^\circ$, though centre on a direction nearly perpendicular to the strike of the slope. Therefore, accretion was lateral to somewhat oblique relative to the formative current on average.

Within D2, Figure 15 shows that the dune crests had less diverse orientations centred 30° from the slope-perpendicular direction. The clinoforms would have been oblique-laterally accreting.

Within D3 (north flank), the clinoform-like surface was smoother but smaller superimposed dunes can be observed in Figure A1d, with a transition on its west side to a train of larger dunes. In that time-lapse sequence, dunes are difficult to associate between surveys but they are asymmetric with east-facing lee slopes suggesting that they migrated to the east as expected from tidal models (Fairley et al., 2016). Figure 15 shows that dune crests were oriented sub-perpendicular (within ~15°) to the clinoform strike so it also accreted oblique-laterally.

Instead of using the local dune orientations to represent the current directions, the regional trend of the ridge could be used, as modelling shows us that residual currents mostly run parallel to it (Fairley et al., 2016). In that case, the clinoform in D1 apparently accreted at 30° and that at D2 by ~5° to the ridge trend, in both cases obliquely accreting. In the case of D3, however, accretion towards NNW had a component against the direction of the expected current to the ESE (i.e., partly backwards accreting). The sense of accretion therefore varies depending on the scale of observation. However, tidal bars in the ancient rock record are rarely complete, making the regional trend of the ridge difficult to assess reliably, so the comparison of accretion directions with local dune orientations is most useful. Accretion was lateral to oblique at that local scale.

Interpretations

Sand volume changes

We explore here the changes in sand volume shown in Figure 12 and their links to changes in ridge morphology, aided by the general directions of bedload movements shown in Figure 12c, which were interpreted from dune migrations revealed by the time-lapse surveying (Figure A1a). During the 2003 to 2010 interval, the sand extracted commercially (3.5 X 10^6 m^3) was more than 50% larger than the decrease in volume for area E3. From the dune migration pattern, the sand accounting for this discrepancy most likely originated from westward transport on the south side of Nash Sands, turning around the end of the ridge as shown in other tidal ridges (McCave and Langhorne, 1982). If, for the sake of argument, West Nash were considered a separate sedimentary system and we ignore sand supply from further east of it, the sand volume eroded from E2 minus the sand volume deposited at D2 nearly equals the discrepancy (this difference in volume is 1.1 X 10^6 m^3).

The 2003 to 2010 volume change of the whole ridge was +2.9 X 10^6 m^3. Combined with the commercial extraction, that volume change implies that around 6.4 X 10^6 m^3 of sand moved onto the ridge over the observed period. Although the dune movements suggest there was net sand flux to SE into Nash Passage (the area northeast of D5 marked 'c' in Figure 12c), which may have contributed to this change, the dune movements near to the coast (north of D4) were mostly to the NW away from Nash Sands (marked 'b'). There, NW migrating dunes were also revealed by comparing single-beam soundings collected in 2003 with the 2002 multibeam data (Schmitt, 2006). Harris and Collins (1988) estimated a westerly sand flux of 5770 t m^{-1} y^{-1} using transport equations and the current velocity data collected in 1983 at site CM2 south of Nash Point (Figure 2). Could that sand flux partly explain the accumulation on Nash Sands? Multibeam data in Mitchell et al. (2012a) show a sand stream with dunes ~300 m across overlying bedrock near to CM2. If we use a 300-m width of sand flow along with the Harris and Collins (1988) flux and a dry sand density of 1600 kg m^{-3} (www.vcalc.com), we estimate a westward transport of ~7.6 X 10^6 m^3 over 7 years, nearly equal to the 6.4 X 10^6 m^3 sand accumulation. From these estimates, we suggest that Nash Sands is being continually supplied with sand from further east and is not a closed system.

Although the sand broadly circulated in the clockwise pattern expected from model residual current predictions (Fairley et al., 2016), the general NW migration of dunes in the swatchway was not predicted by those models. That migration may help explain the accumulation in D3 (Figure 12c). The specific bedload transport flux (Q in m^2 y^{-1}) associated with the dune migrations can be estimated from fcH, where c is the dune celerity, H is dune height and f is a shape factor commonly taken to have the value 0.6 (Van den Berg, 1987). Using H=1.56 m and c=55.3 m y^{-1} for the dunes marked with bold grey lines in Figure 11, we estimate Q=51.5 m^2 y^{-1}. Multiplying that value by the ~1000 m width of the swatchway suggests ~51 X 10^3 m^3 y^{-1} were transported to D3 through the swatchway. As the dunes in Figure 11 do not form continuous trains, this is an overestimate (Branß et al., 2019) but, on the other hand, we are omitting other forms of transport such as suspended load or bedload not associated with dune movements (Smith, 1988a; Schmitt and Mitchell, 2014). This 51 X 10^3 m^3 y^{-1} compares favourably with 87 X 10^3 m^3 y^{-1} average annual change for D3 so it likely was a significant contributor to the sand accumulated in D3. (This interpretation of the ridge in D3 is similar to that of R. W. Dalrymple (pers. comm. 2020) of a delta-like feature at the northern end of a swatchway in Cobequid Bay, eastern Canada shown by Dalrymple et al. (1990, their Figure 15). Data from there also showed comparable lateral migration of a swatchway of 2.1 km over a 35-year period (Dalrymple et al., 2012).) Agreeing with the preceding discussion of volume changes in areas D2-E3, we suggest that little sand crossed the Nash swatchway from East Nash to join the West Nash circulation during 2003-2010.

Processes occurring in the swatchway (E2 and D1)

We interpret the two migration directions within the swatchway (to NW and NNW) as arising from different currents in different parts of the tidal cycle. The NW current would have arisen when the ebb flow was rapidly streaming (the NW facing dunes are essentially continuations of the southerly flank dunes, expected to be active during ebb streaming), whereas the NNW current may have arisen towards ebb slack water. Pattiaratchi and Collins (1984) demonstrated the importance of storm waves to sand transport within Swansea Bay and Giardino et al. (2010) demonstrated how waves can affect the magnitude and direction of sand flux over shelf sand ridges. Surface waves are therefore likely to have enhanced transport in the swatchway around slackwater by maintaining stresses more continually above the sand threshold of motion and by providing a component of stress on the bed in the wave propagation direction, typically towards the NE. (Depths in the maps shown here are relative to water level at lowest astronomical tide, so the swatchway depths were only ~3-10 m around spring low spring tides (C4 and C5 in Figure 7) and ~2 m deeper during neap tides.) The NNW current would require that a water pressure gradient developed across the Nash Sands during the ebb phase to cause it, whereas the opposite current during the flood phase was not strong enough to reverse these dune migrations.

Although numerical modelling is required to explore this fully, a few effects can be speculated to contribute to the swatchway current. First, an influence may arise from water surface stress due to winds, which predominantly approach from the SW. Pingree and Griffiths (1980) estimated by modelling that such currents would be a few cm s^{-1} northwards across the entrance to the Bristol Channel. Intermittent winds, however, do not obviously explain the nearly constant rates of dune migration in Figure 11 and the predicted currents are small, so wind stress most likely has only a minor effect. Second, rapid ebb flow past the Nash Point headland could lead to reduced flow through Nash Passage and over East Nash compared with the flood tide via the mechanisms of flow asymmetry and momentum that have been proposed (Pingree, 1978; Ferentinos and Collins, 1980; Heathershaw and Hammond, 1980; Dyer and Huntley, 1999; Yin et al., 2003; Berthot and Pattriaratchi, 2006b; Neill and Scourse, 2009). Measurements from a current meter installed immediately north of East Nash at "T3" in Figure 2 in the 1970s recorded only 4 hours of ebb tide compared with 8 hours of the slower flood tide and the ebb current was ~20° clockwise from that expected of a rectilinear reversal of the flood current (Ferentinos and Collins, 1980). With reduced water supply from up-estuary, the water surface north of Nash Sands may therefore have declined in elevation more rapidly than that south of Nash Sands. A similar explanation was given for swatchway currents in Cobequid Bay, Bay of Fundy (Dalrymple et al., 1990). Third, besides the north-south ridge at UTM 453 km east, 5699 km north, the seabed north of Nash Sands is less rugged than that south of Nash Sands, where rock outcrops have a relief of 2-3 m. For a similar difference in bedform relief in the Torres Strait, Hughes et al. (2008) estimated from current meter data the coeffícent C_D relating bed shear stress due to tidal currents to the square of current speed. Their results showed a 6% greater coefficient over the larger bedforms. Although this value is modest, similarly smaller friction coefficients to the north of Nash Sands would assist the more rapid escape of water in the north during ebb phases.

Secondary currents have been speculated to have a role in sand ridge development and maintenance (Caston and Stride, 1970). Although not now considered important for linear open-shelf ridges, they have been recorded at headlands (Geyer, 1993). Berthot and Pattriaratchi (2005; 2006a) also reported secondary currents next to a headland-associated sand ridge. Such currents are found in rivers at meander bends, where the water surface becomes tilted by centrifugal effects, so that the difference in hydrostatic pressure at the river bed causes a component of near-bed flow perpendicular to the down-stream flow and towards the inner meander bank (Bridge, 2003). We might expect similar secondary currents to form during ebb flow around the steep SW margin of East Nash, causing a near-bed current component towards the NE, assisted by Coriolis force also acting to the right of the main current (Neill, 2008). Although secondary currents are typically an order of magnitude smaller than the main flow (Heathershaw and Hammond, 1980; Berthot and Pattriaratchi, 2005), they may help to explain why a major sand volume did not cross the swatchway from East to West Nash during the period of observations. The orientations of dunes at the base of the SW margin of East Nash (D1) and on the north flank of the D3 promontory (Figure 15) therefore likely reflect the vector sum of the main flow and secondary currents.

Sand was partly delivered to D1 by the dune train in E1, which narrows strongly going westwards towards D1 (Figure 2). The 19-day depth change in Figure 13d shows deposition in the lee slopes of the dunes of up to 5 m indicating rapid fluxes. Annualised flux estimated from the dune heights H of ~2 m, dune train width of ~160 m, 19-day translations of ~10 m and form factor f of 0.6 using the procedure as before was 37000 m^3 y^{-1}. That flux was about a factor of five or more less than the annualised volume change in D1, so some sand may also have been carried west by sheet flow, by migrations of unresolved bedforms or by the flood tidal currents over the crest of East Nash. The crestal platform is shallow, rising above chart datum in places. Within the 1-m-resolution data shown in Figure 13, small megaripples can be observed superimposed on the southern flank dunes and on the SW-facing flank lacking dunes further west. However, the megaripples are absent or less well-resolved towards the lip of the platform. We speculate that waves breaking along the southern edge of the platform during ebbing or low tide may have played a role by continually resuspending sand, which was carried westwards by the strong ebb current and that wave breaking is responsible for the smoother uppermost flank.

Down-slope of the area of proposed breaking waves in D1, the clinoform-like sheets may have been emplaced by grain flow assisted by ebb currents and/or by wave-assisted gravity currents as described by Flores et al. (2018) in similar water depths but in shallower gradients of only ~0.3°.

Longer-term changes in ridge geomorphology

UK Admiralty charts dating from 1949 reveal that the area around the swatchway has varied in morphology greatly, with the 10-m depth contour marking the SE limit of West Nash appearing to move along the ridge by as much as 1800 m from 1949 to 1980-1993 (Schmitt, 2006). Figure 16 shows bathymetry changes in a dense grid of single-beam data collected over the ridge from 1991 to 2002 (Lewis et al., 2015). It shows modest changes from 1991 to 1997, followed by rapid deposition at D1 over 1997-1998, which was then followed by erosion at D1 over 1998-2001. The bathymetry data are shown as a time-lapse map series in Figure A1e. Those maps show the ridge was persistently weakly sinuous in plan-view over those 13 years. If we identify the three main inflections by D1-D3 in the more recent morphology (Figure 12c), those inflections varied in location. Inflections D2 and D3 migrated slowly towards the WNW from 1991 to 1997, abruptly moved ESE 1997-1998 and then moved to the WNW again by 2001. In 1991 and 1992, the ridge was sinuous but had no clear swatchway or saddle along its length. From those years to 2002, the sinuous shape became more accentuated with a shallow swatch or saddle appearing in 1993.

Lewis et al. (2015) showed that variations in cross-sectional shape of the ridge at D1 were correlated with wave conditions. Their calculations suggested that oscillating currents due to waves in 1999 and 2000 exceeded the sand threshold of motion over Nash Sands for 20% more of the time than in 1997 and 1998. During that 1999-2000 period, erosion occurred in area D1. Thus, waves as well as the processes outlined earlier are likely to have played a strong role in shaping the ridge. The swatchway morphology has developed largely as the SW margin of East Nash has become more prominent, so the swatchway development discussed below may indirectly be linked to how waves have affected the cross-sectional form of the ridge as Lewis et al. (2015) described.

Discussion

Development of cross-stratified beds of large thickness

Within the lower clinothems, migrations of megaripples and effects of the subordinate tides may have left a more complex stratigraphy than we show in Figures 6 and 14. However, as the dunes generally translated relatively simply (Figures A1b-A1d), cross-stratified beds potentially developed in areas D1 and D2. In Figure 6, the cross-stratified beds are significantly thick compared with the heights of the dunes. Simple geometrical modelling by Rubin and Hunter (1982) suggested that such a development would be unusual. They wrote that, during deposition of cross-stratification beds, "Because sediment is thus transferred from bedforms to underlying strata, bedforms must decrease in cross-sectional area or in number, or both, unless sediment lost from bedforms during deposition is replaced with sediment transported from outside the depositional area." Within D1 and D2, dunes do not appear to decline in height down residual currents rapidly enough to explain the deposition (Figures A1b-A1c), so sediment is likely indeed transported from outside the parts of the profiles where the cross-stratification developed. Within area D1, the sediment was probably supplied in suspension by sediment gravity flows down the SW flank of East Nash and/or ebb tidal currents as we have suggested. For area D2, the origin of the sediment is less clear as the crest of the bank is shallower and thus less exposed to waves. The movements of dunes north of the crest of the bank in the time-lapse bathymetry map (Figure A1a) suggest that flood tidal currents carried some sand to the crest, so that may have been an additional source.

Development of swatchways

Following the work of Caston (1972) based on hydrographic sounding data from the southern North Sea, there has been general interest in how swatchways develop and whether they represent stages when sand ridges divide. He suggested that small irregularities along the flanks of linear ridges could become amplified by the sand streams (dune trains) on either flank, leading to sand-ridge kinks that exaggerate until the ridges become S-shaped in plan-view. In his model, those inflections could then ultimately “blow out” creating swatchways and leaving the ridges forming a series of smaller autonomous ridges. Caston’s (1972) model was prompted by emergence of a swatchway in a ridge offshore Ramsgate (UK) over a period exceeding 100 years (Cloet, 1954) and partly supported by observations of progressive accentuation of a kink in one ridge (Ower) in the area studied by him. In contrast, Smith (1988b), studying historical hydrographic soundings of a kinked sand ridge in the Netherlands North Sea, found no evidence for such an evolution. He suggested that a process was needed to cause a local decline in the ridge elevation for a swatchway to form, either by reduced supply of sand to the incipient swatchway or shallowing of the crests of the ridge to either side of the incipient swatchway. In his model, large dunes are important stores of sand, locally restricting sand movement.

Although numerical models of sand ridge evolution can produce plan-view irregularities somewhat replicating Caston's (1972) model (Yuan and de Swart, 2017; Yuan et al., 2017; van Veelen et al., 2018), that replication could be fortuitous. Detailed current and sand transport observations needed to support modelling of sand movements around ridge kinks and swatchways are still limited. The Nash Sands findings somewhat support the ideas of Smith (1988b) locally. The swatchway was maintained for a decade by a net NW-directed cross-ridge sand transport and possibly by secondary currents associated with the prominent flank at D1. Both effects helped to prevent transport to E2, thus leading to erosion there, allowing the westward migration of the swatchway.

The extent to which these mechanisms develop kinks generally in open-shelf sand ridges (Caston, 1972) is less clear. Deleu et al. (2004) reported a detail study of a kink area of a 26-km-long open-shelf ridge in the Belgian North Sea. Bathymetry data collected over different years revealed only a slow migration onto the ridge's steeper lee side and no major change in the bathymetric depression at the kink. Sediment transport modelling based on a depth-averaged tidal current model without wave effects predicted greater transport rates over the shallower crests of the ridge away from the kink, hence not obviously explaining how the kink area could deepen. They suggested that any development of a swatchway would require other mechanisms such as those proposed by Smith (1988b). In contrast with their results, Garel (2010) showed data from repeated transects with a hull-mounted acoustic Doppler current profiler (ADCP) across an artificially deepened area of another ridge, which suggested divergent sand transport within the depression and thus potential to create a swatchway, although those observations were limited to only seven tidal cycles. Development of a swatchway off the east coast of the UK (through Cross Sand) appears to be partly explained by divergent residual currents, predicted using a depth-averaged tidal model, and a function of how the tide interacts with the broader geomorphology (Horrillo-Caraballo and Reeve, 2008). The greater tendency for swatchways to develop in nearshore ridges (Cloet, 1954; Horrillo-Caraballo and Reeve, 2008) compared with the open-shelf ridges (Deleu et al., 2004) could ultimately reflect how differential water levels develop by the interaction of the tide with complex seabed geometry in shallow coastal areas, as suggested for swatchways in Nash Sands here and for Cobequid Bay by Dalrymple et al. (1990).

<u>Preservation of stratigraphy in modern offshore sand ridges and in outcrops</u>

We discuss here the longer-term evolution of Nash Sands and also consider the stratigraphy of other tidal sand ridges in modern and ancient settings. Nash Sands is highly mobile, so the clinoforms of Figure 6 may survive only decades, but clinoforms have been imaged with seismic reflection methods in tidal ridges and bars, including in swatchways (Dalrymple and Zaitlin, 1994; Dalrymple and Rhodes, 1995), so they represent a class of sedimentary feature that can be preserved. In particular, the clinoforms in D1 (Figure 6a), are reminiscent of dipping reflections in seismic data shown by Dalrymple and Rhodes (1995, their figure 13-31), likely also produced by accretion on one side of a swatchway. Channels crossing tidal-strait sand ridges in south Italian outcrops have also been interpreted as swatchways (Longhitano et al., 2021). The regions between the 10 m contours in East and West Nash away from the swatchway were more stable. Beneath the layer of sand that is repeatedly mobilised by migrating dunes in these areas, Nash Sands likely has a stable core that should contain stratigraphy reflecting its earlier development.

Dyer and Huntley (1999) described banner banks as potentially evolving as their associated headlands retreat, such as because of erosion or with relative sea level rise (their Type 3B banks). If sufficiently rapid and the stratigraphy buried by later sediments, such retreat could in principle lead to stratigraphy being preserved. Snedden and Dalrymple (1998) suggested that tidal ridges are most likely to be preserved in transgression sequences of ancient successions, as suggested by seismic reflection imaging on outer shelves (Yang, 1989; Berné et al., 2002). Headland extension could lead to banner banks becoming moribund and their stratigraphy preserved. In principle, rapid headland extension or generation could occur with relative sea-level fall, tectonics (uplift of a fault escarpment), massive landsliding or volcanic emplacements. Willis (2005) also suggested changes in sediment supply to tidal bars could lead to abandonment and Suter (2006) mentioned rapid sea-level rise as potentially leading to preservation of tidal ridges, an effect implicit in the rapid subsidence of Michaud and Dalrymple (2016). In contrast, some researchers have described tidal-strait sand ridges preserved by tectonic uplift and hence relative sea-level fall (Leszczyński and Nemec, 2020; Longhitano et al., 2021).

Seismic images collected perpendicular to tidal sand ridges commonly include reflection sequences dipping sub-parallel to their modern dipping flanks, i.e., clinoforms (Houbolt, 1968; Berné et al., 1993; Berné et al., 1994; Reynaud et al., 1999; Trentesaux et al., 1999; Bastos et al., 2003; Chaumillon et al., 2013; Franzetti et al., 2015). These suggest recent evolution by progressive deposition of sand on the ridge flanks and is observed locally here (Figure 7). However, other parts of those seismic data also commonly show more complex stratigraphy with depositional surfaces dipping in both directions and erosional surfaces. Whereas many sand ridges are created by deposition, some may be created by erosion of pre-existing deposits (Berné et al., 1998; Jin and Chough, 2002). The Nash Sands clinoforms in Figure 6 illustrate how rapidly such features can form, here over decades, only a small fraction of the likely millennial lifetimes of tidal sand ridges.

<u>Interpreting stratigraphic records of ancient tidal ridge outcrops</u>

The processes operating during the life times of tidal ridges and bars and their ultimate fates have been addressed through a combination of active monitoring (e.g. time-lapse bathymetric data, as here), sampling and geophysical surveys (Berné et al., 1994; Berné et al., 1998; Fenies and Taslet, 1998; Reynaud et al., 1999; Trentesaux et al., 1999; Vecchi et al., 2013; Franzetti et al., 2015; Lockhart et al., 2018), hydrodynamic modelling (De Vriend, 1990; Hulscher et al., 1993; van Veelen et al., 2018) and analyses of ancient examples preserved in cored subsurface sections (Folkestad and Satur, 2008; Schwarz et al., 2011; Messina et al., 2014; Wei et al., 2018; Chiarella et al., 2020) and in the rock record (Tillman and Martinsen, 1984; Gaynor and Swift, 1988; Mellere and Steel, 1995; Martinsen et al., 1999; Yoshida, 2000; Plink-Björklund and Steel, 2006; Plink-Björklund, 2008; Steel et al., 2008; Pontén and Plink-Björklund, 2009; Hampson, 2010; Michaud, 2011; Martinius, 2012; Olariu, M. et al., 2012; Scasso et al., 2012; Steel et al., 2012; Chen et al., 2014; López et al., 2016; Michaud and Dalrymple, 2016; Sharafi et al., 2016; Leszczynski and Nemec, 2020; Longhitano et al., 2021). The latter potentially provide the finest spatial information but, before assessing it, we need to be confident that tidal ridges or bars have been correctly identified. Lateral accretion (deposition in inclined layers in directions perpendicular to the tidal currents) has been a key characteristic used to discriminate tidal ridges or bars from other tidal structures, in particular from dune complexes, which are expected instead to comprise forward accreting clinoforms (Harris, 1988; Stride, 1988; Anastas et al., 1997; Dalrymple, 2010; Longhitano et al., 2012b; Olariu, C. et al., 2012; Reynaud and Dalrymple, 2012). Harris et al. (1992) described sets of foreset beds in cores taken from the centres of some sand ridges in a bay mouth shoal complex, apparently caused by climbing dunes. They were also forward accreting, so accretion style is not unequivocal evidence, although it is the most easily assessed in outcrops.

Michaud and Dalrymple (2016) interpreted eight sandstone bodies of the Eocene Roda Formation in Spain as banner or headland-associated banks. As these are the best reported outcrop examples of banner banks, it is interesting to compare them with modern examples. In particular, they noted a large scatter in the current directions derived from cross-stratification. Megaripples on Nash Sands have reliefs of ~10-20 cm and their crestlines are commonly oriented differently from their host dunes and are commonly more diversely oriented (Schmitt and Mitchell, 2016). Hence, assessment of current directions needs to focus on only the larger (>20 cm) beds that can be more confidently assigned to dunes, which was the case in the Roda Formation study (Michaud, 2011). The Nash Sands results show areas of lateral accretion 1-4 km in extent (measured along clinoform strikes), whereas the majority of the ridge by area did not significantly accrete over the duration of the observations. This lack of extensive lateral accretion is likely a general feature of banner banks attached to persistent headlands where there is less scope for lateral movements compared with open-shelf banks (Reynaud and Dalrymple, 2012). The dune crest orientations in Figure 15 are varied in D1, but less varied in D2 and D3. The strong influence of waves at Nash Sands and its sinuous morphology may not correspond to the environment and morphology of the Roda Formation sand bodies studied by Michaud and Dalrymple (2016). However, the variability in current directions there is comparable with that of dune crestline orientations at Nash Sands. The Roda Formation ridges may therefore similarly have had more complex and time-varying forms than the simple elongate ridges that Michaud and Dalrymple (2016) were able to infer from the rock exposures.

We have surveyed the literature on modern banner or headland-associated banks to see if there are common features that might be diagnostic for interpreting outcrop successions. We found eight relatively simple ridges without swatchways or major breaks in their summits (Duffy and Hughes-Clarke, 2005; Berthot and Pattriaratchi, 2006a; Neill et al., 2007; Schmitt et al., 2007; Neill, 2008; Shaw et al., 2012; Li et al., 2014; Coni e Mello et al., 2019; McCarroll et al., 2020). In contrast, ridges either side of Portland Bill (Bastos et al., 2002; Bastos et al., 2004) and west of Cape d'Or, Bay of Fundy (Shaw et al., 2012) are accompanied by second ridges or shoals, which Shaw et al. (2012) called "shadow banks". The former may originate from changing geomorphology with sea-level rise (Neill and Scourse, 2009), whereas the latter may have a hydrodynamic origin (Shaw et al., 2012). Some ridges more remote from headlands but showing swatchways or strong segmentation include Kenfig Patches, Swansea Bay (Harris, 1988) and Goodwin Sands (Cloet, 1954). The plan-view S-shape of Nash Sands is therefore unusual.

The large variability in banner bank morphology likely relates to diverse tidal and wave current regimes associated with their different settings and seabed geomorphology, so it is not easy to generalise. Interpretation of ancient tidal ridges needs to consider this variability of morphology and process.

Can stratigraphy be related to changes in wave climate and storm surges?

Although we have imperfect environmental data, the potential benefit of comparing the stratigraphic development from time-lapse surveys with environmental changes can be evaluated. According to Figure 3b, the more extreme waves were ~20% larger in height through the winters of 2006/2007 and 2007/2008 than 2005/2006 or 2008/2009. From the water elevation maxima in Figure 3c, storm surges were greatest in spring and autumn of 2006. Surges take several tidal cycles to evolve and have been predicted to strongly enhance the peak magnitudes of tidal currents and affect their directions around Nash Sands, in turn affecting sand movements (Fairley et al., 2016). We compare the erosion and deposition rates of Figure 12b to the environmental data from late 2007 onwards, when the multibeam survey dates are better known and hence rates of volume change are more accurate.

From Figure 12b, the stratigraphy within D1 developed steadily, with somewhat faster accumulation in the 2007/08 winter of extreme waves. Deposition was then slower in the second half of 2008 and summer of 2009 when extreme waves were smaller, before rising again in 2010 when waves were still subdued but storm surges may have enhanced currents (Figure 3c). Somewhat similar features can be observed for D2 and D3. However, erosion was enhanced at E1-E4 over the period of less extreme waves (2008-2009). Lower extreme waves appear to have led to a reduction in volume of Nash Sands as a whole. This suggests that waves do not merely enhance sand transport by ensuring that the bed shear stress is above the sand threshold of motion, but also affects how much sand is exchanged with the seabed surrounding Nash Sands.

Furthermore, while volume accumulation rates generally peaked over the 2007/2008 winter, it did so curiously at different times (West Nash E2, D2 and E3 in late 2007 and East Nash D3, E4, D4, D5 and E1 in early 2008). From the data in Figure 12b, the late 2007 accumulations on West Nash were not obviously at the expense of East Nash. Potentially, sand was therefore added to West Nash from elsewhere, such as from the surrounding seabed.

In contrast, correlations between changes in profile shape of Nash Sands and wave conditions were found by Lewis et al. (2015). Erosion occurred in D1 during 1998-2001 (Figure 16), an interval of stronger wave conditions (Lewis et al., 2015). Reactivation (erosional) surfaces are commonly found in tidal sand sequences within cross-bedding produced by dune migrations (Dalrymple and Choi, 2007; Dalrymple, 2010; Longhitano et al., 2012a). They have been interpreted as forming during slack water conditions (Longhitano et al., 2012b) or during the subordinate (reversed) tide (Dalrymple, 2010). From the Lewis et al. (2015) results and modelling of this (Fairley et al., 2016) and other tidal systems (Amos et al., 1995), reactivation surfaces in dune-produced cross-bedding within tidal ridge sequences could also be created during times of extreme wave and/or storm surge activity (Reynaud and Dalrymple, 2012). We interpret our 2007-2010 observations as suggesting that such features could further also have complex origins from changes in the ridge morphology affecting the tidal currents as well as environmental conditions, hence their simple interpretation from field outcrops may not be possible.

<u>Recommendations for time-lapse surveying of tidal sand ridges</u>

Although assessing stratigraphic development would clearly benefit from using modern systems, for example, kinematic GPS to resolve vessel vertical position due to tides, achieving more continuous monitoring over a large area of a tidal ridge would be difficult, given that each survey typically took a few weeks. In contrast, the monitoring of a delta front by Hughes Clarke et al. (2016) was possible with daily surveys as the area was small. We have found that different parts of Nash Sands varied over different timescales. The gross morphology in this study and flank dune movements measured by Schmitt (2006) were largely captured with annual surveys. However, the movements of the small base-of-clinoform dunes (Figure 6) were not well captured with six-monthly surveys; three monthly or shorter seems to be required. The laterally discontinuous beds at the crest of the ridge may have been created from even more mobile bedforms and may require monthly surveys.

To capture the migrations of bedforms adequately requires the bedforms to be recognisable between surveys, but bedforms can change shape in plan-view and profile, affected by surface waves, the ellipticity of the tidal currents and other factors. Based on the experience here and elsewhere (van Landeghem et al., 2012; Schmitt and Mitchell, 2014), we suggest that surveying needs to be repeated at least within intervals over which bedforms migrate by no more than one quarter of a bedform spacing, if bedforms are to be recognized confidently. Hence, if R is the local bedform migration rate and λ the bedform spacing, we recommend surveying at time intervals of $\lambda/4R$.

Surveys of tidal ridge systems ought to be carried out initially with two reconnaissance surveys closely spaced in time to capture the typical velocities of different components. Later surveys can then be planned with more frequent surveying of rapidly changing areas and less frequent surveying of slowly changing areas. We also recommend carrying out the surveys as far as possible using common survey track lines, as this allows a more thorough error analysis of the survey data over immobile benchmarks, since uncertainties vary with beam angle as well as depth (Schmitt et al., 2008).

Conclusions

This study of data from 13 surveys carried out over 8 years has revealed three areas of net deposition where inflections of Nash Sands migrated along the ridge. The stratigraphy generated in those areas comprised three clinothems, each including, in their lower parts, thin cross-beds from dune migrations overlain by a unit of parallel dipping or sigmoidal clinoforms. (Migrating megaripples and effects of subsidiary tidal currents, which cannot be observed from these data, will have complicated the stratigraphy in practice.) Clinoform top-sets were mostly removed by erosion and overlain by a cap of spatially limited irregular beds. Comparing the orientations of dune crests with the strike of the apparent clinoforms in the clinotherms, all three cases involved oblique-lateral accretion locally.

Within one depositional area, dune migrations led to climbing cross-stratified beds with cross-sets almost as thick as the heights of originating dunes.

As the formative dune train did not show rapid decelerations or reductions in height down-stream, we interpret this unusual occurrence as a result of sediment supplied to the dunes in suspension from the adjacent flank of East Nash, which compensated for volume loss due to deposition (Rubin, 1987). Such suspended sediment likely originated from waves observed breaking along the southerly side of East Nash. This highlights the importance of understanding sediment transport components in three-dimensions when interpreting the origins of thick cross-beds generally.

The swatchway separating West and East Nash contained NW-migrating dunes, which explain the build-up of sediment across the north of the swatchway (D3). We speculate that the current causing that migration arose from a lower water level north of Nash Sands during ebb conditions, with sand transport likely enhanced by waves, particularly when water level was lower towards slack water. This effect of different tidal levels may be a common feature of the development of swatchways in nearshore sand ridges (Cloet, 1954; Dalrymple et al., 1990; Horrillo-Caraballo and Reeve, 2008). In the case of Nash Sands, a study of volume changes suggests that westward transport stopped or was significantly reduced at the swatchway, perhaps due to secondary currents developed where the strong ebb tide turned sharply around East Nash into the swatchway. Furthermore, the change in volume of Nash Sands minus the sand extracted commercially is roughly equal to the estimated westerly transport of $\sim 7.6 \text{ X } 10^6 \text{ m}^3$ over 7 years immediately south of Nash Point. This balance suggests that Nash Sands is being continually supplied with sand from further east and is not a closed system. Furthermore, sand volume changes on West and East Nash peaked at different times, suggesting that West Nash was supplied by sand from the area surrounding the west part of the ridge as well.

We have found modest relationships between the development of the stratigraphy and wave conditions or storm surges, with a near-synchronous accumulation on Nash Sands during times of elevated extreme waves through the winter of 2007/08 and a near-synchronous decline in sand over the winter of 2008/09, when extreme waves were lower. In contrast, Lewis et al. (2015) found significant erosion at D1 during stronger wave conditions for the decade earlier. While this requires modelling to investigate further, these contrasting results suggest a complex behaviour. Details of stratigraphy in ancient tidal sand ridges need to be interpreted with caution, as deposition may not be simply related to wave conditions, for example, but also depend on how the evolving morphology of each ridge affects the tidal currents locally.

Acknowledgements

We thank the companies (Hanson Aggregates Marine, Tarmac Marine Dredging and CEMEX UK Marine) who funded the acquisition of these multibeam sonar data and allowed them to be used for this study, as well as the vessel crew and surveyors who carried out the data collection. We are grateful to Matt Lewis for passing on to us the single beam soundings used for Figure 16. Thierry Schmitt is thanked for helping to acquire and process the 2002 multibeam data, which were collected with grants from the NERC (NER/E/S/2001/00408) and HEFCW (NER/F/S/20/00/00146) as well as funding from the above companies. Most of the figures in this article were produced with the GMT software system (Wessel and Smith, 1991). Zhongwei Zhao is thanked for extracting the ERA wave properties in Figure 3. We are particularly grateful to reviewers Bob Dalrymple and Peter Harris, and associate editor Jaco Baas, for insightful comments and observations that significantly improved this article. The authors declare they have no conflicts of interest.

Data sharing and accessibility

The 2002 multibeam sonar data can be made available by reasonable request to the first author. The other multibeam data are proprietary and not publicly available, although digital versions of the derived profiles (Figures 6 and 7) can be made available by reasonable request. The current velocity data in Figure 2a and tide gauge data in Figure 2c can be obtained from the British Oceanographic Data Centre (www.bodc.ac.uk). The wave information in Figure 2b can be obtained from the European Centre for Medium-Range Weather Forecasts (www.ecmwf.int).

References

Ahmadian, R., Olbert, A.I., Hartnett, M. and Falconer, R.A. (2014) Sea level rise in the Severn Estuary and Bristol Channel and impacts of a Severn Barrage. *Comput. Geosc.*, **66,** 94-105.

Allen, J.R.L. (1980) Sand waves: a model of origin and internal structure. *Sed. Geol.*, **26,** 281-328.

Amos, C.L., Barrie, J.V. and Judge, J.T. (1995) Storm-enhanced sand transport in a macrotidal setting, Queen Charlotte Islands, British Columbia, Canada. *Spec. Publs. Int. Ass. Sed.*, **54,** 53-68.

Anastas, A.S., Dalrymple, R.W., James, N.P. and Nelson, C.S. (1997) Cross-stratified calcarenites from New Zealand: subaqueous dunes in a cool-water, Oligo-Miocene seaway. *Sedimentology*, **44,** 869-891.

Bastos, A., Collins, M.B. and Kenyon, N. (2003) Morphology and internal structure of sand shoals and sandbanks off the Dorset coast, English Channel. *Sedimentology*, **50,** 1105-1122.

Bastos, A., Kenyon, N. and Collins, M.B. (2002) Sedimentary processes, bedforms and facies, associated with a coastal headland: Portland Bill, Southern UK. *Mar. Geol.*, **187,** 235-258.

Bastos, A., Paphitis, D. and Collins, M.B. (2004) Short-term dynamics and maintenance processes of headland-associated sandbanks: Shambles Bank, English Channel, UK. *Est. Coast. Shelf Sci.*, **59,** 33-47.

Belderson, R.H., Johnson, M.A. and Kenyon, N.H. (1982) Bedforms. In: *Offshore tidal sands: processes and deposits* (Ed A.H. Stride), pp. 27-57. Chapman & Hall, London.

Berné, S., Castaing, P., De Batist, M. and Lericolais, G. (1993) Morphology, internal structure and reversal of asymmetry of large subtidal dunes in the Gironde Estuary (France). *J. Sed. Petrol.*, **63,** 780-793.

Berné, S., Lericolais, G., Bourillet, J.F. and De Batist, M. (1998) Erosional offshore sand ridges and lowstand shorefaces: Examples from tide- and wave-dominated environments of France. *J. Sed. Res.*, **98,** 540-555.

Berné, S., Trentesaux, A., Stolk, A., Missiaen, T. and De Batist, M. (1994) Architecture and long term evolution of a tidal sandbank: The Middelkerke Bank (southern North Sea). *Mar. Geol.*, **121,** 57-72.

Berné, S., Vagner, P., Guichard, F., Lericolais, G., Liu, Z., Trentesaux, A., Yin, P. and Yi, H.I. (2002) Pleistocene forced regressions and tidal sand ridges in the East China Sea. *Mar. Geol.*, **188,** 293-315.

Berthot, A. and Pattriaratchi, C. (2005) Maintenance of headland-associated linear sandbanks: modelling of secondary flows and sediment transport. *Ocean Dynamics*, **55,** 526-540.

Berthot, A. and Pattriaratchi, C. (2006a) Field measurements of the three-dimensional current structure in the vicinity of a headland-associated linear sandbank. *Cont. Shelf Res.*, **26,** 295-317.

Berthot, A. and Pattriaratchi, C. (2006b) Mechanism for the formation of headland-associated linear sandbanks. *Cont. Shelf Res.*, **26,** 987-1004.

Bosman, A., Casalbore, D., Romagnoli, C. and Chiocci, F.L. (2014) Formation of an 'a'a lava delta: insights from time-lapse multibeam bathymetry and direct observations during the Stromboli 2007 eruption. *Bull. Volcanol.*, **76,** article 838, doi:10.1007/s00445-014-0838-2.

Bosman, A., Romagnoli, C., Madricardo, F., Correggiari, A., Remia, A., Zubalich, R., Fogarin, S., Kruss, A. and Trincardi, F. (2020) Short-term evolution of Po della Pila delta lobe from time lapse high-resolution multibeam bathymetry (2013-2016). *Est. Coast. Shelf Sci.*, **233,** art 106533.

Bourne, S.J. and Willemse, E.J.M. (2001) Elastic stress control on the pattern of tensile fracturing around a small fault network at Nash Point, UK. *J. Struct. Geol.*, **23,** 1753-1770.

Branß, T., Núñez-González, F. and Aberle, J. (2019) Estimation of bedload by tracking supply-limited bedforms. In: *Marine and River Dune Dynamics - MARID VI - 1-3 April 2019* (Eds A. Lefebvre, T. Garlan and C. Winter), pp. 23-28, Bremen, Germany.

Bridge, J.S. (2003) *Rivers and floodplains: forms, processes and sedimentary record*. Blackwell Science, Oxford, 491 pp.

Buijsman, M.C. and Ridderinkhof, H. (2008) Long-term evolution of sand waves in the Marsdiep inlet. I: High-resolution observations. *Cont. Shelf Res.*, **28,** 1190-1201.

Bull, J.M., Gutowski, M., Dix, J.K., Henstock, T.J., Hogarth, P., Leighton, T.G. and White, P.R. (2005) Design of a 3D Chirp sub-bottom imaging system. *Mar. Geophys. Res.*, **26,** 157-169.

Caires, S. and Sterl, A. (2003) Validation of ocean wind and wave data using triple collocation. *J. Geophys. Res.*, **108,** Paper C3098, doi:10.1029/2002JC001491.

Caston, V.N.D. (1972) Linear sand banks in the southern North Sea. *Sedimentology*, **18,** 63-78.

Caston, V.N.D. and Stride, A.H. (1970) Tidal sand movement between some linear sand banks in the North Sea off northeast Norfolk. *Mar. Geol.*, **9,** M38-M42.

Chaumillon, E., Féniès, H., Billy, J., Breilh, J.-F. and Richetti, H. (2013) Tidal and fluvial controls on the internal architecture and sedimentary facies of a lobate estuarine tidal bar (The Plassac Tidal Bar in the Gironde Estuary, France). *Mar. Geol.*, **346,** 58-72.

Chen, S., Steel, R.J., Dixon, J.F. and Osman, A. (2014) Facies and architecture of a tide-dominated segment of the Late Pliocene Orinoco Delta (Morne L'Enfer Formation) SW Trinidad. *Mar. and Pet. Geol.*, **57,** 208-232.

Chiarella, D., Longhitano, S.G., Mosdella, W. and Telesca, D. (2020) Sedimentology and facies analysis of ancient sand ridges: Jurassic Rogn Formation, Trøndelag Platform, offshore Norway. *Mar. Pet. Geol.*, **112,** article 104082.

Cloet, R.L. (1954) Hydrographic analysis of the Goodwin Sands and the Brake Bank. *Geographical Journal*, **120,** 203-215.

Collins, M.B. (1987) Sediment transport in the Bristol Channel: a review. *Proceedings of the Geologists' Association*, **98,** 367-383.

Collins, M.B. and Ferentinos, G. (1984) Residual circulation in the Bristol Channel, as suggested by Woodhead sea-bed drifter recovery patterns. *Oceanol. Acta*, **7,** 33-42.

Coni e Mello, A.C., Landim Dominguez, J.M. and Pereira de Souza, L.A. (2019) The Santo Antônio Bank: a high-resolution seismic study of a deflected ebb-tidal delta located at the entrance of a large tropical bay, eastern Brazil. *Geo-Mar. Lett.*, **40,** 965-975.

Dalrymple, R.W. (1984) Morphology and internal structure of sandwaves in the Bay of Fundy. *Sedimentology*, **31,** 365-382.

Dalrymple, R.W. (2010) Tidal depositional systems. In: *Facies Models* (Eds N.P. James and R.W. Dalrymple), **4**, pp. 201-231. Geological Association of Canada, St. John's, Newfoundland & Labrador, Canada.

Dalrymple, R.W. and Choi, K. (2007) Morphologic and facies trends through the fluvial-marine transition in tide-dominated depositional systems: A schematic framework for environmental and sequence-stratigraphic interpretation. *Earth-Sci. Rev.*, **81,** 135-174.

Dalrymple, R.W., Knight, R.J., Zaitlin, B.A. and Middleton, G.V. (1990) Dynamics and facies model of a macrotidal sand-bar complex, Cobequid Bay-Salmon River Estuary (Bay of Fundy). *Sedimentology*, **37,** 577-612.

Dalrymple, R.W., Mackay, D.A., Ichaso, A.A. and Choi, K.S. (2012) Processes, morphodynamics, and facies of tide-dominated estuaries. In: *Principles of Tidal Sedimentology* (Eds J. R. A. Davis and R.W. Dalrymple), pp. 79-107. Springer Science+Business Media B.V., New York.

Dalrymple, R.W. and Rhodes, R.N. (1995) Estuarine dunes and bars. In: *Geomorphology and sedimentology of estuaries* (Ed G.M.E. Perillo), pp. 359-422. Elsevier Science.

Dalrymple, R.W. and Zaitlin, B.A. (1994) High-resolution sequence stratigraphy of a complex, incised valley succession, Cobequid Bay - Salmon River estuary, Bay of Fundy, Canada. *Sedimentology*, **41,** 1069-1091.

De Vriend, H.J. (1990) Morphological processes in shallow tidal seas. In: *Residual Currents and Long-term Transport Number 38 in Coastal and Estuarine Studies.* (Ed R.T. Cheng), pp. 276–301. Springer, New York.

Dee, D.P., Uppala, S.M., Simmons, A.J., Berrisford, P., Poli, P., Kobayashi, S., Andrae, U., Balmaseda, M.A., Balsamo, G., Bauer, P., Bechtold, P., Beljaars, A.C.M., Berg, L.v.d., Bidlot, J., Bormann, N., Delsol, C., Dragani, R., Fuentes, M., Geer, A.J., Haimberger, L., Healy, S.B., Hersbach, H., Hólm, E.V., Isaksen, L., Kållberg, P., Köhler, M., Matricardi, M., McNally, A.P., Monge-Sanz, B.M., Morcrette, J.-J., Park, B.-K., Peubey, C., Rosnay, P.d., Tavolato, C., Thépaut, J.-N. and Vitart, F. (2011) The ERA-Interim reanalysis: configuration and performance of the data assimilation system. *Q. J. R. Meteorol. Soc.*, **137,** 553-597.

Deleu, S., Van Lancker, V., Van den Eynde, D. and Moerkerke, G. (2004) Morphologic evolution of the kink of an offshore tidal sandbank: the Westhinder Bank (Southern North Sea). *Cont. Shelf Res.*, **24,** 1587-1610.

Duffy, G.P. and Hughes-Clarke, J.E. (2005) Application of spatial cross correlation to detection of migration of submarine sand dunes. *J. Geophys. Res.*, **110,** article F04S12, doi:10.1029/2004JF000192.

Dyer, K.R. and Huntley, D.A. (1999) The origin, classification and modelling of sand banks and ridges. *Cont. Shelf Res.*, **19,** 1285-1330.

Ernsten, V.B., Noormets, R., Hebbeln, D., Bartholomä, A. and Flemming, B.W. (2006) Precision of high-resolution multibeam echo sounding coupled with high-accuracy positioning in a shallow water coastal environment. *Geo-Mar. Lett.*, **26,** 141-149.

Evans, D.J. and Thompson, M.S. (1979) The geology of the central Bristol Channel and the Lundy area, South Western Approaches, British Isles. *Proc. Geol. Assoc.*, **90,** 1-14.

Fairley, I., Masters, I. and Karunarathna, H. (2016) Numerical modelling of storm and surge events on offshore banks. *Mar. Geol.*, **371,** 106-119.

Fenies, H.G. and Taslet, J.-P. (1998) Facies and architecture of an estuarine tidal bar (the Trompeloup bar, Gironde Estuary, SW France). *Mar. Geol.*, **150,** 149-169.

Ferentinos, G. (1978) *Hydrodynamic and sedimentation processes in Swansea Bay and along the central Northern Bristol Channel coastline*. PhD, University of Wales, Swansea, Swansea.

Ferentinos, G. and Collins, M.B. (1979) Tidally induced secondary circulations and their associated sedimentation processes. *J. Oceanogr. Soc. Jap.*, **35,** 65-74.

Ferentinos, G. and Collins, M.B. (1980) Effects of shoreline irregularities on a rectilinear tidal current and their significance in sedimentation. *J. Sed. Petrol.*, **50,** 1081-1094.

Flores, R.P., Rijnsburger, S., Meirelles, S., Horner-Devine, A.R., Souza, A.J., Pietrzak, J.D., Henriquez, M. and Reniers, A. (2018) Wave generation of gravity-driven sediment flows on a predominantly sandy seabed. *Geophys. Res. Lett.*, **45,** 7634-7645.

Folkestad, A. and Satur, N. (2008) Regressive and transgressive cycles in a rift-basin: Depositional model and sedimentary partitioning of the Middle Jurassic Hugin Formation, Southern Viking Graben, North Sea. *Sed. Geol.*, **207,** 1-21.

Franzetti, M., Le Roy, P., Garlan, T., Graindorge, D., Sukhovich, A., Delacourt, C. and Le Dantec, N. (2015) Long term evolution and internal architecture of a high-energy banner ridge from seismic survey of Banc du Four (Western Brittany, France). *Mar. Geol.*, **369,** 196-211.

Garel, E. (2010) Tidally-averaged currents and bedload transport over the Kwinte Bank, Southern North Sea. *J. Coast. Res.*, **51,** 87-94.

Gaynor, G.C. and Swift, D.J.P. (1988) Shannon sandstone depositional model: sand ridge dynamics on the Campanian Western Interior shelf. *J. Sed. Petrol.*, **58,** 868-880.

Geyer, W.R. (1993) Three-dimensional tidal flow around headlands. *J. Geophys. Res.*, **98,** 955-966.

Giardino, A., Van den Eynde, D. and Monbaliu, J. (2010) Wave effects on the morphodynamic evolution of an offshore sand bank. *J. Coast. Res.*, **special issue 51,** 127-140.

Gibbard, P.L., Hughes, P.D. and Rolfe, C.J. (2017) New insights into the Quaternary evolution of the Bristol Channel, UK. *J. Quat. Sci.*, **32,** 564-578.

Guiastrennec-Faugasa, L., Gillet, H., Jacinto, R.S., Dennielou, B., Hanquiez, V., Schmidt, S., Simplet, L. and Rousset, A. (2020) Upstream migrating knickpoints and related sedimentary processes in a submarine canyon from a rare 20-year morphobathymetric time-lapse (Capbreton submarine canyon, Bay of Biscay, France). *Mar. Geol.*, **423,** article 106143.

Hage, S., Cartigny, M.J.B., Clare, M.A., Sumner, E.J., Vendettuol, D., Clarke, J.E.H., Hubbard, S.M., Talling, P.J., Lintern, D.G., Stacey, C.D., Englert, R.G., Vardy, M.E., Hunt, J.E., Yokokawa, M., Parsons, D.R., Hizzett, J.L., Azpiroz-Zabala, M. and Vellinga, A.J. (2018) How to recognize crescentic bedforms formed by supercritical turbidity currents in the geologic record: Insights from active submarine channels. *Geology*, **46,** 563-566.

Haine, C. (2000) *Bristol Channel marine aggregates: Resources and constraints research project (company report)*. Postford Duvivier and ABP MER.

Hamilton, E., Watson, P.J., Cleary, J.J. and Clifton, R.J. (1979) The geochemistry of recent sediment in the Bristol Channel - Severn Estuary System. *Mar. Geol.*, **31,** 139-182.

Hampson, G.J. (2010) Sediment dispersal and quantitative stratigraphic architecture across an ancient shelf. *Sedimentology*, **57,** 96-141.

Harris, P.T. (1988) Large-scale bedforms as indicators of mutually evasive sand transport and the sequential infilling of wide-mouthed estuaries. *Sed. Geol.*, **57,** 273-298.

Harris, P.T. and Collins, M.B. (1985) Bedform distributions and sediment transport paths in the Bristol Channel and Severn Estuary, U.K. *Marine Geology*, **62,** 153-166.

Harris, P.T. and Collins, M.B. (1988) Estimation of annual bedload flux in macrotidal estuary: Bristol Channel, UK. *Mar. Geol.*, **83,** 237-252.

Harris, P.T. and Collins, M.B. (1991) Sand transport in the Bristol Channel - bedload parting zone or mutually evasive transport pathways. *Marine Geol.*, **101,** 209-216.

Harris, P.T., Pattiaratchi, C.B., Cole, A.R. and Keene, J.B. (1992) Evolution of subtidal sandbanks in Moreton Bay, eastern Australia. *Mar. Geol.*, **103,** 225-247.

Heathershaw, A.D. and Hammond, F.D.C. (1980) Secondary circulations near sand banks and in coastal embayments. *Deutsche Hydrografische Zeitschrift*, **33,** 135-151.

Heijnen, M.S., Clare, M.A., Cartigny, M.J.B., Talling, P.J., Hage, S., Lintern, D.G., Stacey, C., Parsons, D.R., Simmons, S.M., Chen, Y., Sumner, E.J., Dix, J.K. and Hughes Clarke, J.E. (2020) Rapidly-migrating and internally-generated knickpoints can control submarine channel evolution. *Nature Comm.*, **11,** art. 3129.

Hizzett, J.L., Hughes Clarke, J.E., Sumner, E.J., Cartigny, M.J.B., Talling, P.J. and Clare, M.A. (2018) Which triggers produce the most erosive, frequent, and lognest runout turbidity currents on deltas? *Geophys. Res. Lett.*, **45,** 855-863.

Horrillo-Caraballo, J.M. and Reeve, D.E. (2008) Morphodynamic behaviour of a nearshore sandbank system: The Great Yarmouth Sandbanks, U.K. *Mar. Geol.*, **254,** 91-106.

Houbolt, J.J.H.C. (1968) Recent sediments in the Southern Bight of the North Sea. *Geol. en Mijnbouw*, **47,** 245-273.

Hughes Clarke, J.E. (2016) First wide-angle view of channelized turbidity currents links migrating cyclic steps to flow characteristics. *Nature Communications*, **7,** art 11896, doi:10.1038/ncomms11896.

Hughes, M.G., Harris, P.T., Heap, A. and Hemer, M.A. (2008) Form drag is a major component of bed shear stress associated with tidal flow in the vicinity of an isolated sand bank, Torres Strait, northern Australia. *Cont. Shelf Res.*, **28,** 2203-2213.

Hulscher, S.J.M.H., de Swart, H.E. and De Vriend, H.J. (1993) The generation of offshore tidal sand banks and sand waves. *Cont. Shelf Res.*, **13,** 1183-1204.

Huthnance, J.M. (1982a) On one mechanism forming linear sand banks. *Estuarine, Coastal and Shelf Science*, **14,** 79-99.

Huthnance, J.M. (1982b) On the formation of sand banks of finite extent. *Estuarine, Coastal and Shelf Science*, **15,** 277-299.

Jennings, S.C., Orford, J.D., Canti, M., Devoy, R.J.N. and Straker, V. (1998) The role of relative sea-level rise and changing sediment supply on Holocene gravel barrier development: the example of Porlock, Somerset, UK. *The Holocene*, **8,** 165-181.

Jin, J.H. and Chough, S.K. (2002) Erosional shelf ridges in the mid-eastern Yellow Sea. *Geo-Mar. Lett.*, **21,** 219-225.

Kelner, M., Migeon, S., Tric, E., Couboulex, F., Dano, A., Lebourg, T. and Taboada, A. (2016) Frequency and triggering of small-scale submarine landslides on decadal timescales: Analysis of 4D bathymetric data from the continental slope offshore Nice (France). *Marine Geol.*, **379,** 281-297.

Knaapen, M.A.F., Henegouw, C.N.v.B. and Hu, Y.Y. (2005) Quantifying bedform migration using multi-beam sonar. *Geo-Mar. Lett.*, **25,** 306-314.

Kostaschuk, R. and Best, J. (2005) Response of sand dunes to variations in tidal flow: Fraser Estuary, Canada. *J. Geophys. Res.*, **110,** article F04S04, doi:10.1029/2004JF000176.

Leszczyński, S. and Nemec, W. (2020) Sedimentation in a synclinal shallow-marine embayment: Coniacian of the North Sudetic Synclinorium, SW Poland. *The Depositional Record*, **6,** 144-171.

Lewis, M.J., Neill, S.P. and Elliott, A.J. (2015) Interannual variability of two offshore sand banks in a region of extreme tidal range. *J. Coastal Res.*, **31,** 265-275.

Li, M.Z., Shaw, J., Todd, B.J., Kostylev, V.E. and Wu, Y. (2014) Sediment transport and development of banner banks and sandwaves in an extreme tidal system: Upper Bay of Fundy, Canada. *Cont. Shelf Res.*, **83,** 86-107.

Lloyd, A.J., Savage, R.J.G., Stride, A.H. and Donovan, D.T. (1973) The geology of the Bristol Channel floor. *Phil. Trans Roy. Soc.*, **274,** 595-626.

Lockhart, E.A., Scourse, J.D., Praeg, D., Van Landeghem, K.J.J., Mellett, C., Saher, M., Callard, L., Chiverrell, R.C., Benetti, S., Ó Cofaigh, C. and Clark, C.D. (2018) A stratigraphic investigation of the Celtic Sea megaridges based on seismic and core data from the Irish-UK sectors. *Quat. Sci. Rev.*, **198,** 156-170.

Longhitano, S.G., Chiarella, D., Di Stefano, A., Messina, C., Sabato, L. and Tropeano, M. (2012a) Tidal signatures in Neogene to Quaternary mixed deposits of southern Italy straits and bays. *Sed. Geol.*, **279,** 74-96.

Longhitano, S.G., Mellere, D., Steel, R.J. and Ainsworth, R.B. (2012b) Tidal depositional systems in the rock record: A review and new insights. *Sed. Geol.*, **279,** 2-22.

Longhitano, S.G., Rossi, V.M., Chiarella, D., Mellere, D., Tropeano, M., Dalrymple, R.W., Steel, R.J., Nappi, A. and Olita, F. (2021) Anatomy of a mixed bioclastic-siliciclastic regressive tidal sand ridge: Facies-based case study from the lower Pleistocene Siderno Strait, southern Italy. *Sediimentology*, **in press,** doi: 10.1111/SED.12853.

López, J.L., Ross, V.M., Olariu, C. and Steel, R.J. (2016) Architecture and recognition criteria of ancient shelf ridges; an example from Campanian Almond Formation in Hanna Basin, USA. *Sedimentology*, **63,** 1651-1678.

Marsset, T., Tessier, B., Reynaud, J.-Y., Batist, M.D. and Plagnol, C. (1999) The Celtic Sea banks: an example of sand body analysis from very high-resolution seismic data. *Mar. Geol.*, **158,** 89-109.

Martinius, A.W. (2012) Contrasting styles of siliclastic tidal deposits in a developing thrust-sheet-top basin - the Lower Eocene of the Central Pyrenees (Spain). In: *Principles of Tidal Sedimentology* (Eds J. R.A. Davis and R.W. Dalrymple), pp. 473-506. Springer.

Martinsen, O.J., Ryseth, A., Helland-Hansen, W., Flesche, H., Torkildsen, G. and Idil, S. (1999) Stratigraphic base level and fluvial architecture: Ericson Sandstone (Campanian), Rock Springs Uplift, SW Wyoming, USA. *Sedimentology*, **46,** 235-259.

McCarroll, R.J., Masselink, G., Valiente, N.G., Wiggins, M., Scott, T., Conley, D.C. and King, E.V. (2020) Impact of a headland-associated sandbank on shoreline dynamics. *Geomorph.*, **355,** art. 107065.

McCave, I.N. and Langhorne, D.N. (1982) Sand waves and sediment transport around the end of a tidal sand bank. *Sedimentology*, **29,** 95-110.

McLaren, P., Collins, M.B., Gao, S. and Powys, R. (1993) Sediment dynamics of the Severn Estuary and Inner Bristol Channel. *J. Geol. Soc. Lond.*, **150,** 589-603.

Mellere, D. and Steel, R. (1995) Variability of lowstand wedges and their distinction from forced-regressive wedges in the Mesaverde Group, southeast Wyoming. *Geology*, **23,** 803-806.

Messina, C., Nemec, W., Martinius, A.W. and Elfenbein, C. (2014) The Garn Formation (Bajocian-Bathonian) in the Kristin Field, Halten Terrace: its origin, facies architecture and primary heterogeneity model. *Int. Assoc. Sedimentol. Spec. Publ.*, **46,** 513-550.

Michaud, K.J. (2011) *Facies architecture and stratigraphy of tidal ridges in the Eocene Roda Formation, northern Spain*, Queen's University, Kingston, Ontario, Canada, 137 pp.

Michaud, K.J. and Dalrymple, R.W. (2016) Facies and stratigraphic occurrence of transgressive, headland-attached sand ridges in the Roda Formation, northern Spain. In: *Contributions to Modern and Ancient Tidal Sedimentology: Proceedings of the Tidalites 2012 Conference* (Eds B. Tessier and J.-Y. Reynaud), pp. 313-341. John Wiley & Sons.

Mitchell, N.C. (2005) Channelled erosion through a marine dump site of dredge spoils at the mouth of the Puyallup River, Washington State. *Mar. Geol.*, **220,** 131-151.

Mitchell, N.C., Huthnance, J.M., Schmitt, T. and Todd, B. (2012a) Threshold of erosion of submarine bedrock landscapes by tidal currents. *Earth Surface Processes and Landforms*, **38,** 627-639.

Mitchell, N.C., Masselink, G., Huthnance, J.M., Fernández-Salas, L.M. and Lobo, F.J. (2012b) Depths of modern coastal clinoforms. *J. Sed. Res.*, **82,** 469-481.

Neill, S.P. (2008) The role of Coriolis in sandbank formation due to a headland/island system. *Est. Coast. Shelf Sci.*, **79,** 419-428.

Neill, S.P., Hashemi, M.R. and Elliott, A.J. (2007) An enhanced depth-averaged tidal model for morphological studies in the presence of rotary currents. *Cont. Shelf Res.*, **27,** 82-102.

Neill, S.P. and Scourse, J.D. (2009) The formation of headland/island sandbanks. *Cont. Shelf Res.*, **29,** 2167-2177.

Olariu, C., Steel, R.J., Dalrymple, R.W. and Gingras, M.K. (2012) Tidal dunes versus tidal bars: The sedimentological and architectural characteristics of compound dunes in a tidal seaway, the lower Baronia Sandstone (Lower Eocene), Ager Basin, Spain. *Sedimentary Geology*, **279,** 134-155, doi: 10.1016/j.sedgeo.2012.07.018.

Olariu, M.I., Olariu, C., Steel, R.J., Dalrymple, R.W. and Martinius, A.W. (2012) Anatomy of a laterally migrating tidal bar in front of a delta system: Esdolomada Member, Roda Formation, Tremp-Graus Basin, Spain. *Sedimentology*, **59,** 356-378, doi: 10.1111/j.1365-3091.2011.01253.x.

Owen, A. (1980) The tidal regime of the Bristol Channel: a numerical modelling approach. *Geophys. J. R. Ast. Soc.*, **62,** 59-75.

Pattiaratchi, C.B. and Collins, M.B. (1984) Sediment transport under waves and tidal currents - a case study from the northern Bristol Channel, U.K. *Marine Geol.*, **56,** 27-40.

Pingree, R.D. (1978) The formation of the shambles and other banks by tidal stirring of the seas. *Journal of the Marine Biological Association of U.K.*, **58,** 211-226.

Pingree, R.D. and Griffiths, D.K. (1980) Currents driven by a steady uniform wind stress on the shelf seas around the British Isles. *Oceanol. Acta*, **3,** 227-236.

Plink-Björklund, P. (2008) Wave-to-Tide Facies Change in a Campanian Shoreline Complex, Chimney Rock Tongue, Wyoming-Utah, U.S.A. In: *Recent Advances in Models of Siliciclastic Shallow-Marine Stratigraphy, SEPM Spec. Publ. 90*, pp. 265-291. SEPM (Society for Sedimentary Geology).

Plink-Björklund, P. and Steel, R.J. (2006) Incised valleys on an Eocene coastal plain and shelf, Spitsbergen - part of a linked shelf-slope system. *SEPM Spec. Publ.*, **85,** 281-307.

Pontén, A. and Plink-Björklund, P. (2009) Process regime changes across a regressive to transgressive turnaround in a shelf-slope basin, Eocene central basin of Spitsbergen. *J. Sed. Res.*, **79,** 2-23.

Posamentier, H.W. and Kolla, V. (2003) Seismic geomorphology and stratigraphy of depositional elements in deep-water settings. *J. Sed. Res.*, **73,** 367-388.

Reynaud, J.-Y. and Dalrymple, R.W. (2012) Shallow-marine tidal deposits. In: *Principles of tidal sedimentology* (Eds J. R. A. Davis and R.W. Dalrymple), pp. 335-369. Springer Science+Business Media B.V.

Reynaud, J.-Y., Tessier, B., Proust, J.N., Dalrymple, R., Marsset, T., De Batist, M., Bourillet, J.-F. and Lericolais, G. (1999) Eustatic and hydrodynamic controls on the architecture of a deep shelf sand bank (Celtic Sea). *Sedimentology*, **46,** 703-721.

Robinson, A.H.W. (1960) Ebb-flood channel systems in sandy bays and estuaries. *Geography*, **45,** 183-199.

Rubin, D.M. (1987) *Cross-bedding, bedform, and paleocurrents*. Society of

Economic Paleontologists and Mineralogists, Tulsa, Oklahoma, USA, 187 pp.

Rubin, D.M. and Hunter, R.E. (1982) Bedform climbing in theory and nature. *Sedimentology*, **29,** 121-138.

Scasso, R.A., Dozo, M.T., Cuitiño, J.I. and Bouza, P. (2012) Meandering tidal-fluvial channels and lag concentration of terrestrial vertebrates in the fluvial-tidal transition of an ancient estuary in Patagonia. *Lat. Am. J. Sediment. Basin Analys.*, **19,** 27-45.

Schmitt, T. (2006) *Morphology and dynamics of headland connected sandbanks from high resolution bathymetric surveys: Helwick and Nash Sands, Bristol Channel, UK (PhD thesis)*, Cardiff University (http://ethos.bl.uk/), Cardiff, 218 pp.

Schmitt, T. and Mitchell, N.C. (2014) Dune-associated sand fluxes at the nearshore termination of a banner sand bank (Helwick Sands, Bristol Channel). *Cont. Shelf Res.*, **76,** 64-74.

Schmitt, T. and Mitchell, N.C. (2016) Multibeam survey of a tidal banner bank: morphology of dunes in eroding partially compacted sands? In: *Marine and River Dune Dynamics (MARD) V* (Eds K.J.J. van Landeghem, T. Garlan and J. Baas), pp. 163-166 (http://maridv.bangor.ac.uk/documents/Book_abstracts_MARIDV_2016_000.pdf). Bangor University, North Wales.

Schmitt, T., Mitchell, N.C. and Ramsay, A.T.S. (2007) Use of swath bathymetry in the investigation of sand dune geometry and migration around a near shore 'banner' tidal sandbank. In: *Coastal and shelf sediment transport, Geological Society Lond., Special Publication 274* (Eds P.S. Balson and M.B. Collins), **Spec. Publ. 274**, pp. 53-64. Geological Society, London.

Schmitt, T., Mitchell, N.C. and Ramsay, A.T.S. (2008) Characterizing uncertainties for quantifying bathymetry change between time-separated multibeam echo-sounder surveys. *Cont. Shelf Res.*, **28,** 1166-1176.

Schwarz, E., Veiga, G.D., Spalletti, L.A. and Massaferro, J.L. (2011) The transgressive infill of an inherited-valley system: The Springhill Formation (lower Cretaceous) in southern Austral Basin, Argentina. *Mar. and Pet. Geol.*, **28,** 1218-1241.

Sharafi, M., Longhitano, S.G., Mahboubi, A., Moussavi-Harami, R. and Mosaddegh, H. (2016) Sedimentology of a transgressive mixed-energy (wave/tide-dominated) estuary, Upper Devonian Geirud Formation (Alborz Basin, northern Iran). In: *Contributions to Modern and Ancient Tidal Sedimentology: Proceedings of the Tidalites 2012 conference* (Eds B. Tessier and J.-Y. Reynaud), pp. 255-286. Int. Assoc. Sediment. (Wiley Blackwell), Chichester, UK.

Shaw, J., Todd, B.J., Li, M.Z. and Wu, Y. (2012) Anatomy of the tidal scour system at Minas Passage, Bay of Fundy, Canada. *Mar. Geol.*, **323-325,** 123-134.

Signell, R.P. and Harris, C.K. (2000) Modeling sand bank formation around tidal headlands. In: *Estuarine and Coastal modeling, 6th International Conference, New Orleans* (Ed A.F. Spaulding M.L. and Blumberg).

Smith, D.B. (1988a) Bypassing of sand over sand waves and through a sand wave field in the central region of the Southern North Sea. In: *Tide-influenced sedimentary environments and facies* (Eds P.L. de Boer, A. van Gelder and S.D. Nio), pp. 39-50. D. Reidal Publishing Company, Boston.

Smith, D.B. (1988b) Stability of an offset kink in the North Hinder Bank. In: *Tide-Influenced Sedimentary Environments and Facies* (Eds P.L. de Boer, A. van Gelder and S.D. Nio), pp. 65-78. D. Reidel Publishing Company, Boston.

Snedden, J.W. and Dalrymple, R.W. (1998) Modern shelf sand ridges: From historical perspective to a unified hydrodynamic and evolutionary model. In: *Sequence Stratigraphic Analysis and Sedimentologic Interpretation, SEPM Spec. Publ. 64* (Eds K. Bergman and J.W. Snedden), **64**, pp. 13-28. SEPM

Steel, R.J., Carvajal, C., Petter, A. and Uroza, C. (2008) Shelf and shelf-margin growth in scenarios of rising and falling sea level. In: *Recent Advances in Models of Siliciclastic Shallow-Marine Stratigraphy, SEPM Spec. Publ. 90*, pp. 47-71.

Steel, R.J., Plink-Björklund, P. and Aschoff, J. (2012) Tidal deposits of the Campanian Western Interior Seaway, Wyoming, Utah and Colorado, USA. In: *Principles of Tidal Sedimentology* (Eds J. R.A. Davis and R.W. Dalrymple), pp. 437-471. Springer.

Stride, A.H. (1988) Preservation of marine sand wave structures. In: *Tide-influenced sedimentary environments and facies* (Eds P.L. de Boer, A. van Gelder and S.D. Nio), pp. 13-22. D. Reidal Publishing Company, Boston.

Stride, A.H. and Belderson, R.H. (1990) A reassessment of sand transport paths in the Bristol Channel and their regional significance. *Marine Geol.*, **92,** 227-236.

Stride, A.H. and Belderson, R.H. (1991) Sand transport in the Bristol Channel east of Bull Point and Worms Head: a bed-load parting model with some indications of mutually evasive sand transport paths. *Marine Geol.*, **101,** 203-207.

Stride, A.H., Belderson, R.H., Kenyon, N.H. and Johnson, M.A. (1982) Offshore tidal deposits; sand sheet and sand bank facies. In: *Offshore Tidal Sands: Processes and Deposits* (Ed A.H. Stride), pp. 95-125. Chapman & Hall, London.

Suter, J.R. (2006) Facies models revised: clastic shelves. In: *Facies models revisited, SEPM Special Publication No. 84* (Eds H.W. Posamentier and R.G. Walker), pp. 339-397. SEPM (Society for Sedimentary Geology).

Talling, P.J., Allin, J., Armitage, D.A., Arnott, R.W.C., Cartigny, M.J.B., Clare, M.A., Felletti, F., Covault, J.B., Girardclos, S., Hansen, E., Hill, P.R., Hiscott, R.N., Hogg, A.J., Clarke, J.H., Jobe, Z.R., Malgesini, G., Mozzato, A., Naruse, H., Parkinson, S., Peel, F.J., Piper, D.J.W., Pope, E., Postma, G., Rowley, P., Squazzini, A., Stevenson, C.J., Sumner, E.J., Sylvester, Z., Watts, C. and Xu, J. (2015) Key future directions for research on turbidity currents and their deposits. *J. Sed. Res.*, **85,** 153-169.

Tengberg, A., De Bovee, F., Hall, P., Berelson, W., Chadwick, D., Ciceri, G., Crassous, P., Devol, A., Emerson, S., Gage, J., Glud, R., Graziottini, F., Gundersen, J., Hammond, D., Helder, W., Hinga, K., Holby, O., Jahnke, R., Khripounoff, A., Lieberman, S., Nuppenau, V., Pfannkuche, O., Reimers, C., Rowe, G., Sahami, A., Sayles, F., Schurter, M., Smallman, D., Behrli, B. and De Wilde, P. (1995) Benthic chamber and profiling landers in oceanography - A review of design, technical solutions and functioning. *Progr. Oceanogr.*, **35,** 253-294.

Tillman, R.W. and Martinsen, R.S. (1984) The Shannon shelf-ridge sandstone complex, Salt Creek anticline area, Powder River Basin, Wyoming. In: *Siliclastic Shelf Sediments, SEPM Spec. Publ. 34*, **34**, pp. 85-142. SEPM.

Trentesaux, A., Stolk, A. and Berné, S. (1999) Sedimentology and stratigraphy of a tidal sand bank in the southern North Sea. *Mar. Geol.*, **159,** 253-272.

Uncles, R.J. (1983) Modelling tidal stress, circulation and mixing in the Bristol Channel as a prerequisite for ecosystem studies. *Can. J. Fish. Aqua. Sci.*, **40 (Suppl. 1),** 8-19.

Van den Berg, J.H. (1987) Bedform migration and bed load transport in some rivers and tidal environments. *Sedimentology*, **34,** 681-698.

van Landeghem, K.J.J., Baas, J.H., Mitchell, N.C., Wilcockson, D. and Wheeler, A.J. (2012) Reversed sediment wave migration in the Irish Sea, NW Europe: A reappraisal of the validity of geometry-based predictive modelling and assumptions. *Marine Geol.*, **295-298,** 95-112.

van Veelen, T.J., Roos, P.C. and Hulscher, S.J.M.H. (2018) Process-based modelling of bank-breaking mechanisms of tidal sandbanks. *Cont. Shelf Res.*, **167,** 139-152.

Vecchi, L.G., Aliotta, S., Ginsberg, S.S. and Giagante, D.A. (2013) Morphodynamic behavior and seismostratigraphy of a sandbank: Bahía Blanca estuary, Argentina. *Geomorph.*, **189,** 1-11.

Vendettuoli, D., Clare, M.A., Clarke, J.E.H., Vellinga, A.J., Hizzett, J.L., Hage, S., Cartigny, M.J.B., Talling, P.J., Waltham, D., Hubbard, S.M., Stacey, C.D. and Lintern, D.G. (2019) Daily bathymetric surveys document how stratigraphy is built and its extreme incompleteness in submarine channels. *Earth and Planet. Sci. Letts.*, **515,** 231-247.

Wallingford, H. 2016. Review of aggregate dredging off the Welsh coast, HR Wallingford Ltd.

Wei, X., Steel, R.J., Ravnås, R., Jiang, Z., Olariu, C. and Ma, Y. (2018) Anatomy of anomalously thick sandstone units in the Brent Delta of the northern North Sea. *Sed. Geol.*, **367,** 114-134.

Wessel, P. and Smith, W.H.F. (1991) Free software helps map and display data. *EOS, Transactions, American Geophysical Union*, **72,** 441.

Wienberg, C. and Hebbelm, D. (2005) Impact of dumped sediments on subaqueous dunes, outer Weser Estuary, German Bight, southeast North Sea. *Geo-Mar. Lett.*, **25,** 43-53.

Willis, B.J. (2005) Deposits of tide-influenced river deltas. In: *River deltas - concepts, models, and examples. S.E.P.M. Spec. Publ. 83*, pp. 87-129.

Xu, J.P., Wong, F.L., Kvitek, R., Smith, D.P. and Paull, C.K. (2008) Sandwave migration in Monterey Submarine Canyon, Central California. *Marine Geol.*, **248,** 193-212.

Yang, C.-S. (1989) Active, moribund and buried tidal sand ridges in the East China Sea and the southern Yellow Sea. *Mar. Geol.*, **88,** 97-116.

Yin, J., Chen, Y. and Falconer, R.A. (2003) Steady shallow-water current and solute transport around a semi-conical headland. *Environmental Fluid Mechanics*, **3,** 221-234.

Yoshida, S. (2000) Sequence and facies architecture of the upper Blackhawk Formation and the Lower Castlegate Sandstone (Upper Cretaceous), Book Cliffs, Utah, USA. *Sed. Geol.*, **136,** 239-276.

Yuan, B. and de Swart, H.E. (2017) Effect of sea level rise and tidal current variation on the long-term evolution of offshore tidal sand ridges. *Mar. Geol.*, **390,** 199-213.

Yuan, B., de Swart, H.E. and Panadés, C. (2017) Modeling the finite-height behavior of offshore tidal sand ridges, a sensitivity study. *Cont. Shelf Res.*, **137,** 72-83.

Table 1: Details of survey dates and equipment used.

Survey start[1]	Survey end[2]	Sonar[4]	Position source[5]	Tidal height source[6]	Motion sensor[7]
2002/8/7	2002/9/4	Reson Seabat 8101	DGPS	Valeport	Applanix POS-MV 220
2003/9		Geoswath[3]	DGPS[3]	PT[8]	DMS 05[3]
2004/2		Geoswath[3]	DGPS[3]	PT[8]	DMS 05[3]
2004/8		Geoswath[3]	DGPS[3]	Valeport[3]	DMS 05[3]
2005/2		Geoswath[3]	DGPS[3]	Valeport[3]	DMS 05[3]
2005/6		Geoswath[3]	DGPS[3]	Valeport[3]	DMS 05[3]
2006/6		Geoswath[3]	DGPS[3]	Valeport[3]	DMS 05[3]
2007/7/29	2007/8/10	Geoswath	DGPS	Valeport	DMS 05
2008/2/19	2008/3/19	Geoswath	DGPS	PT	DMS 05
2008/7/1	2008/8/8	Geoswath	KGPS	KGPS	DMS 05
2009/2/12	2009/3/19	Geoswath	KGPS	KGPS	DMS 05
2009/7/9	2009/9/9	Geoswath	KGPS	KGPS	DMS 05
2010/2/11	2010/4/12	Geoswath	KGPS	KGPS	DMS 05

[1]Dates: year/month/day.
[2]If only a start date is given, that date represents the estimated central month of the survey.
[3]Presumed based on other company reports
[4]Geoswath: Geoacoustics Geoswath Plus 250 kHz swath sonar.
[5]DGPS: differential GPS, KGPS: kinematic GPS
[6]Valeport: Midas Water Level Recorder (seabed installed), PT: Port Talbot tide gauge.
[7]DMS 05: TSS (now Teledyne Marine) DMS-05; Applanix POS-MV 220: combined motion and navigation system.
[8]Presumed tide gauge used based on track-parallel errors visible in Figure 4 (upper-left two panels encompassing 2003 Feb to 2004 August).

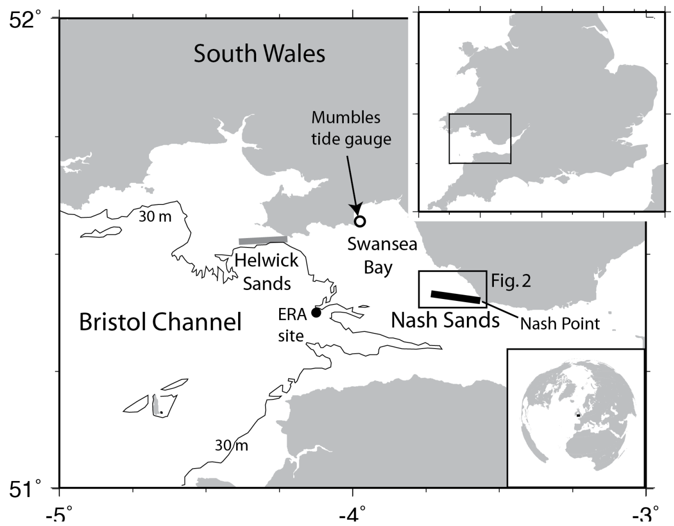

Figure 1. Location of Nash Sands (solid black bar) within the macrotidal Bristol Channel, U.K. (insets locate the main panel). Solid circle marks location used to extract the wave information in Figure 3b. Open circle locates the Mumbles tide gauge, which provided the data in Figure 3c.

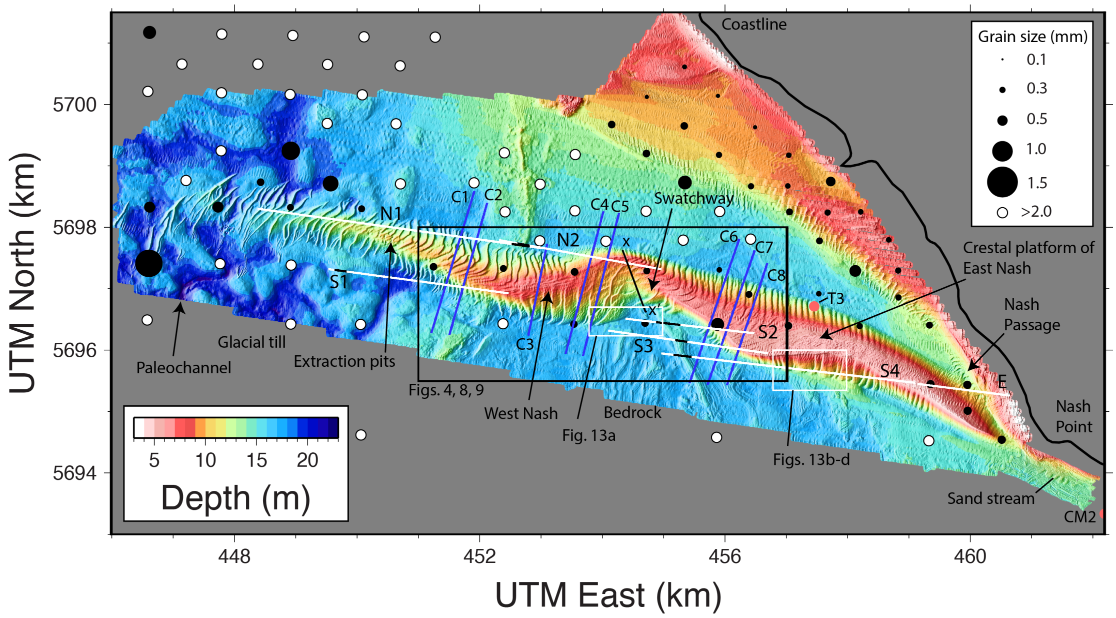

Figure 2. Bathymetry data collected during the August 2008 multibeam survey of Nash Sands (supplemented with multibeam data collected in 2002 around Nash Point). White and blue lines represent cross-sections used to reconstruct stratigraphy in Figures 6 and 7, respectively. Parts of the white lines marked in black represent benchmark assessments of tidal height errors. Red-filled circles locate current meter sites "CM2" of Harris and Collins (1988) (data shown in Figure 3a) and "T3" of Ferentinos and Collins (1980). Grain size data were provided by Haine (2000) (those samples were collected earlier than the multibeam data, hence the morphology has changed and the one coarser sand reading shown may not have originally been collected on the ridge summit). Coordinates are Universal Transverse Mercator (UTM) distances in km (zone 30).

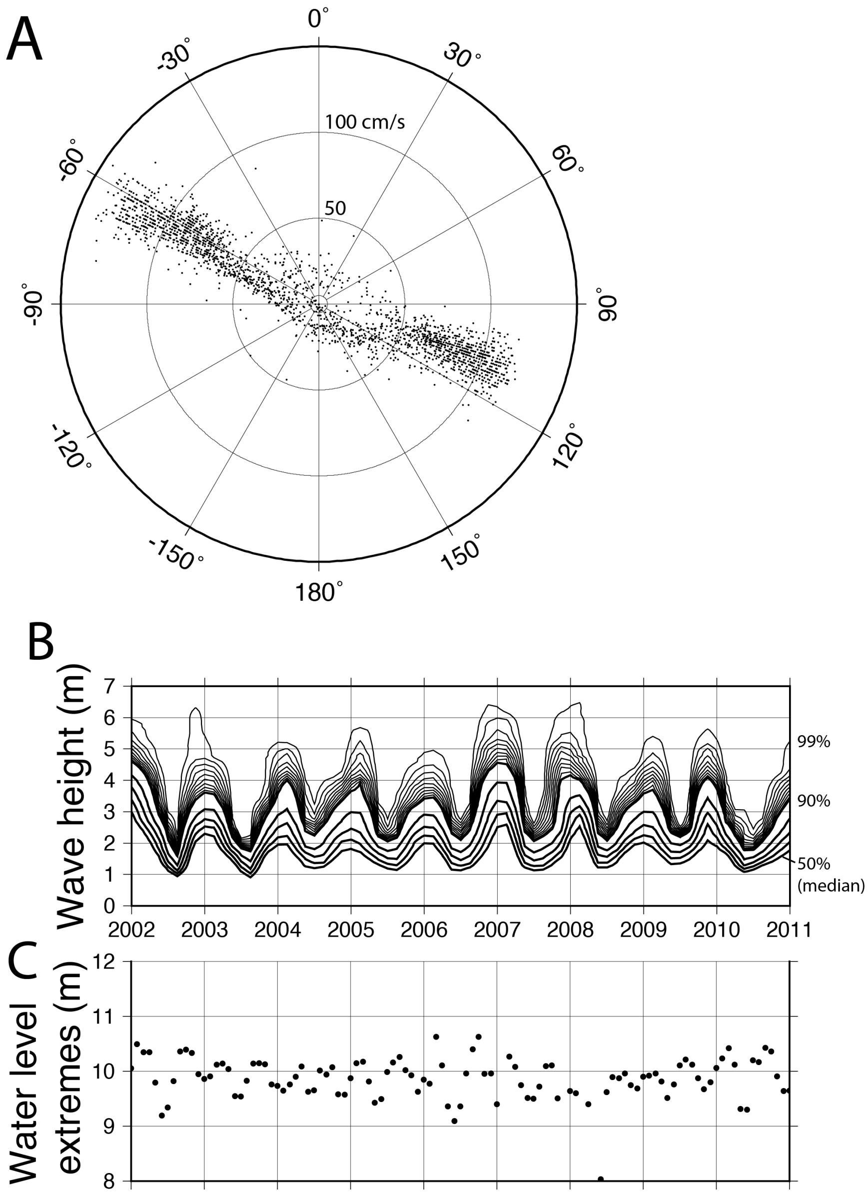

Figure 3: (a) Current velocities measured at site CM2 located in Figure 2 (data from Harris and Collins (1988)). These data were collected by Swansea University scientists with an Aanderaa RCM 4/5 recording current meter moored 2 m above the bed over 16 days (roughly half a spring-neap cycle) and made available by the British Oceanographic Data Centre (www.bodc.ac.uk). Note that the ebb current (to WNW) reaches greater speeds than the flood current (to ESE). (b) Significant wave height during stormy conditions from the ERA-40 and ERA-Interim reanalysis outputs (Caires and Sterl, 2003; Dee et al., 2011) for a position within the Bristol Channel (51.375°N, 4.125°W) located in Figure 1. Bold contours show the median and successively higher 10-percentiles for the 6-hourly wave height estimates binned within 1/4 yearly intervals. Fine contours show each one percentile above 90%. Note the more extreme wave heights during the winters of 2007 and 2008. (c) Maximum water elevation levels relative to Admiralty Chart Datum recorded with a Dataring water level recorder at the Mumbles permanent tide gauge station located in Figure 1 (data courtesy of the National Oceanography Centre, Liverpool licensed under the Open Government Licence v1.0).

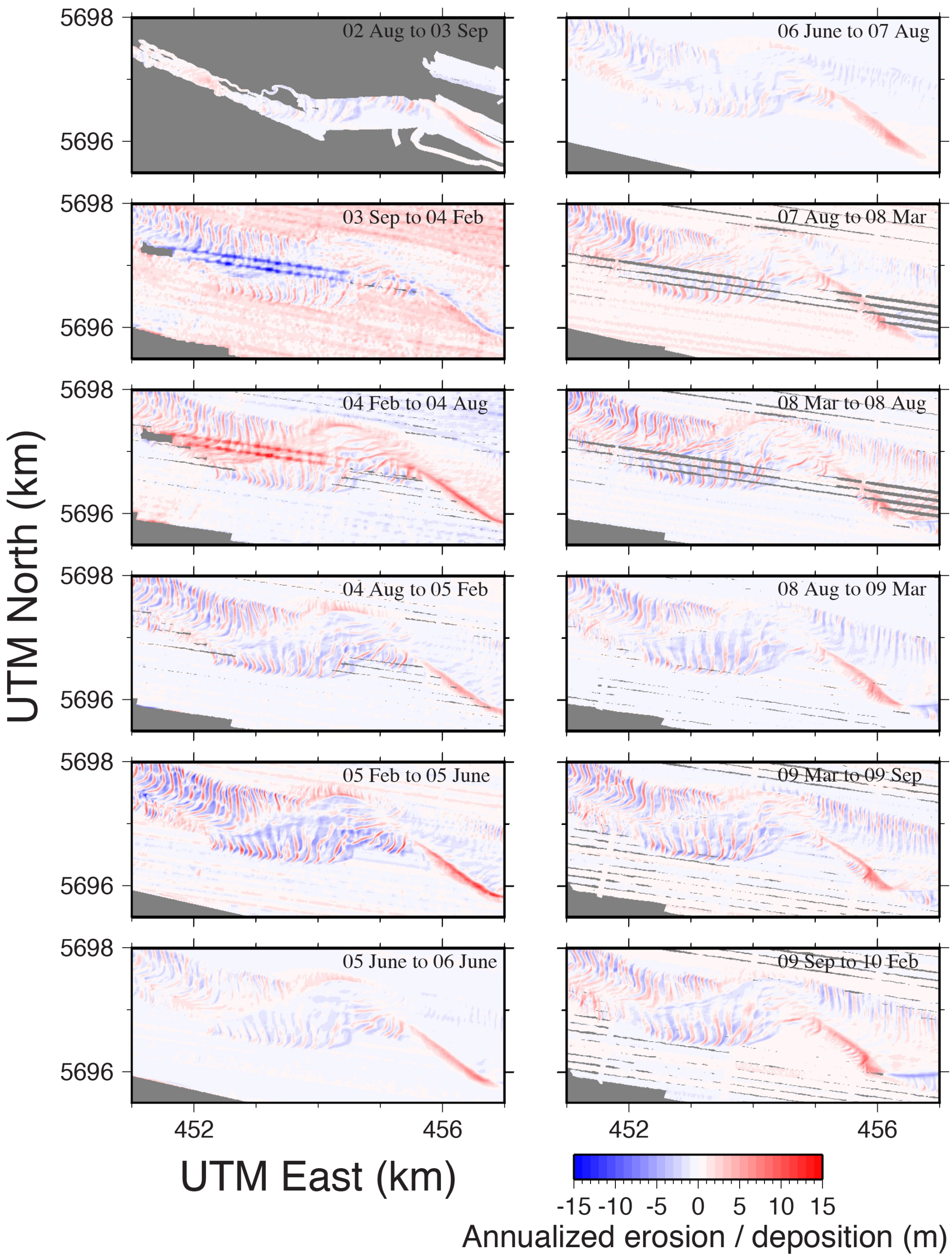

Figure 4. Deposition and erosion derived from pairs of multibeam survey datasets. For ease of interpretation, changes are annualised as time intervals between surveys are unequal. (WNW-ESE lines are artifacts due to either missing survey data (grey bands) or (for upper-left panels spanning February 2003 to August 2004) tidal height errors.)

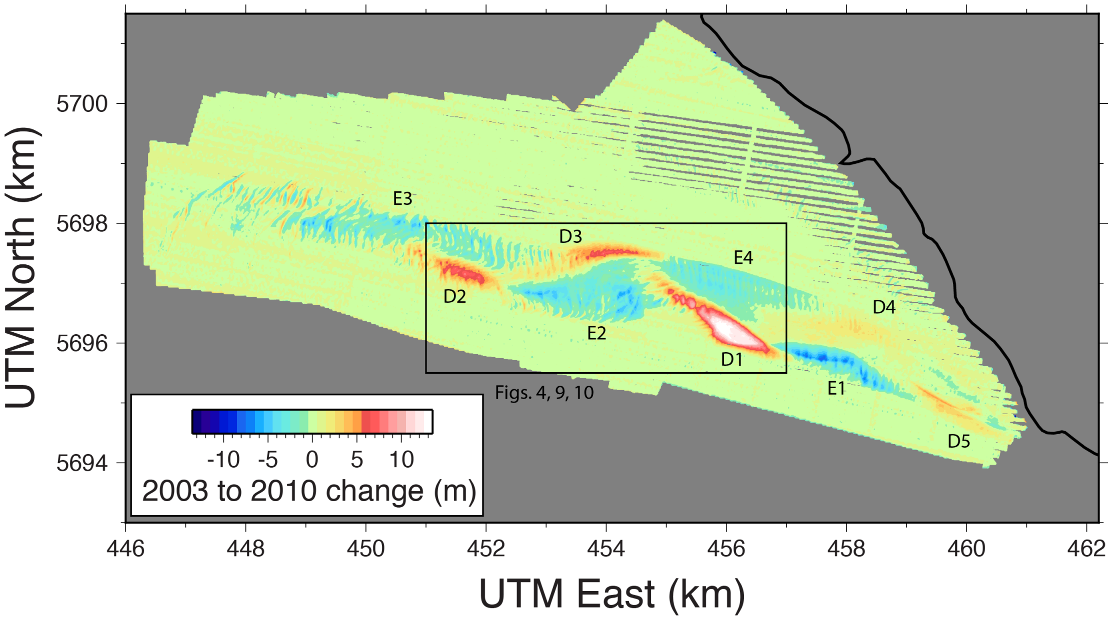

Figure 5. Elevation change over the period September 2003 to February 2010 from the multibeam surveys (positive values represent accretion). Annotation D1-D5 and E1-E4 locate areas of deposition and erosion referred to in the text.

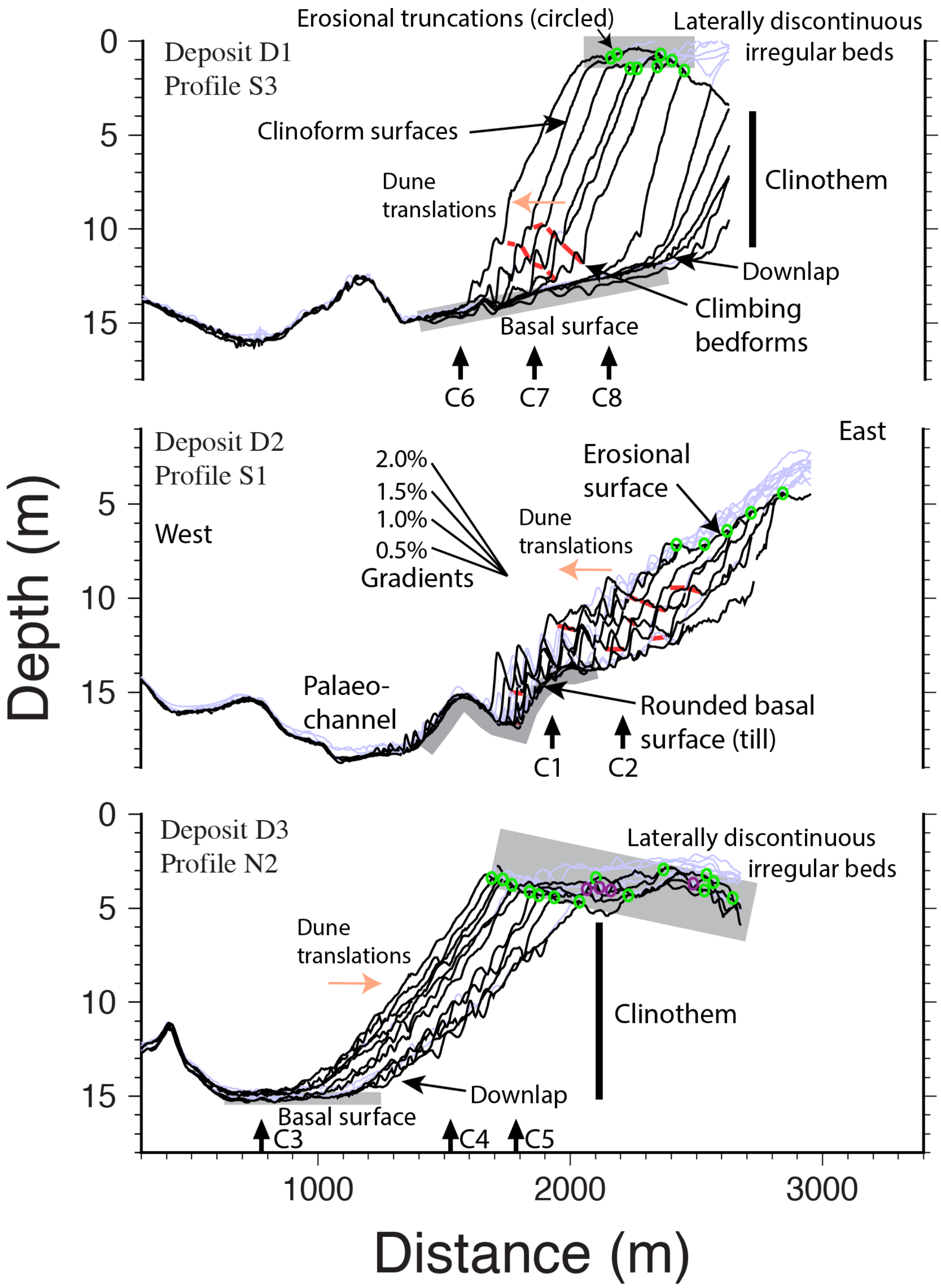

Figure 6. Stratigraphy accumulated within deposit areas D1-D3 to February 2010 along profiles S1, S3 and N2 oriented WNW-ESE and located in Figure 2. Each line represents the results of one multibeam survey. Vertical exaggeration is 75:1. Red bars mark interpreted associations between troughs, i.e., potential bedding surfaces. Green and blue circles highlight erosional truncations of inclined and more nearly horizontal surfaces, respectively. Vertical arrows with annotation C1-C8 locate intersections with the cross-sections in Figure 7. Pink arrows on profiles S1 and S3 indicate sense of dune translations.

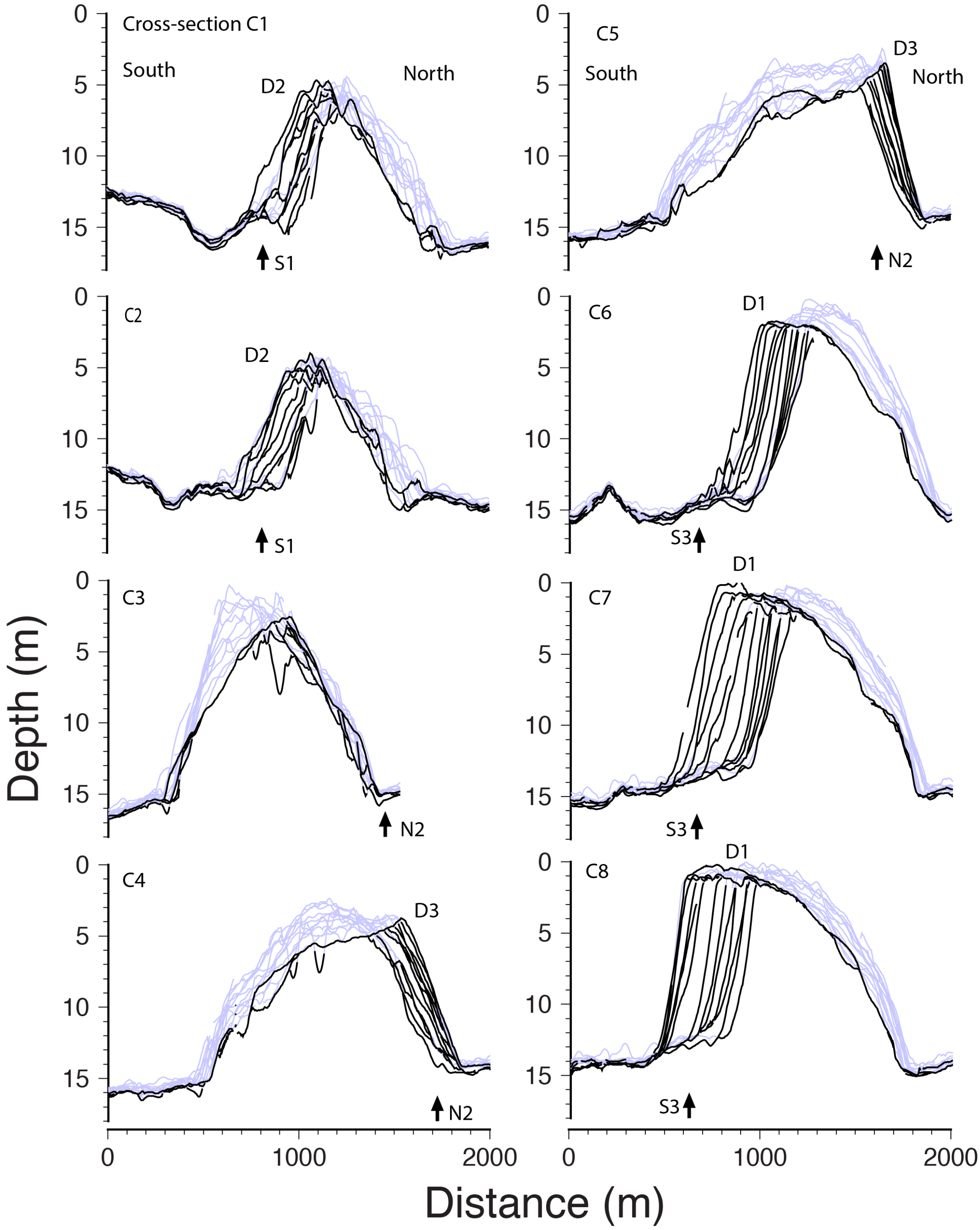

Figure 7. Stratigraphic cross-sections for lines oriented SSW-NNE located in Figure 2. Pale blue lines represent surfaces eroded by the time subsequent surveys took place and black lines represent surfaces remaining by 2010. Arrows with annotation S1, N2 and S3 locate intersections with the longitudinal profiles in Figure 6. Vertical exaggeration is 75:1 (as Figure 6). Annotation D1-D3 represents the deposits located in Figure 12c.

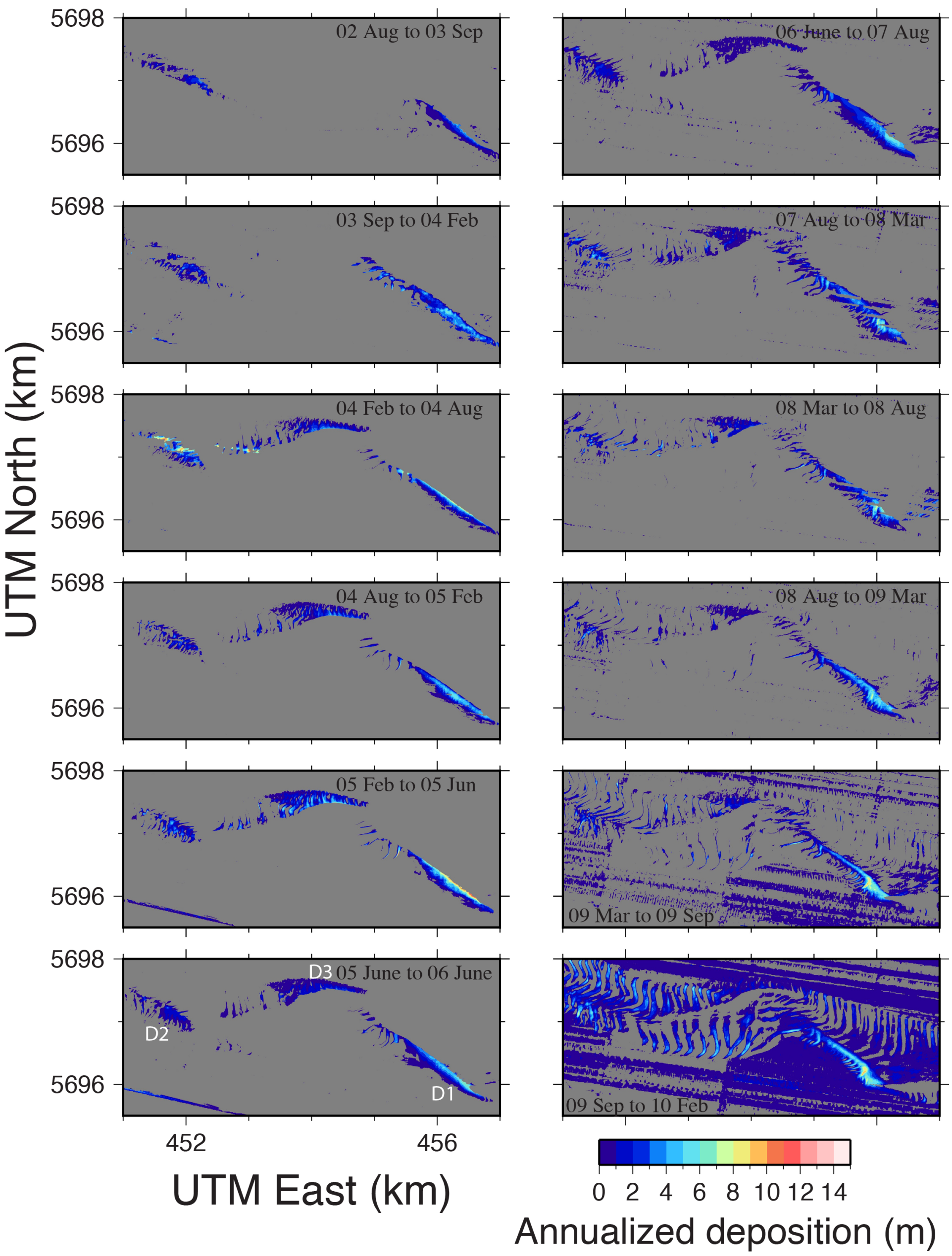

Figure 8. Annualised deposition of the intervals between surveys where not intercepted by later surfaces up until February 2010. This figure is as Figure 4 but with the areas apparently eroded removed and thus represents nearly the pattern of erosion and deposition one would infer if the stratigraphy had been fully mapped and dated in February 2010.

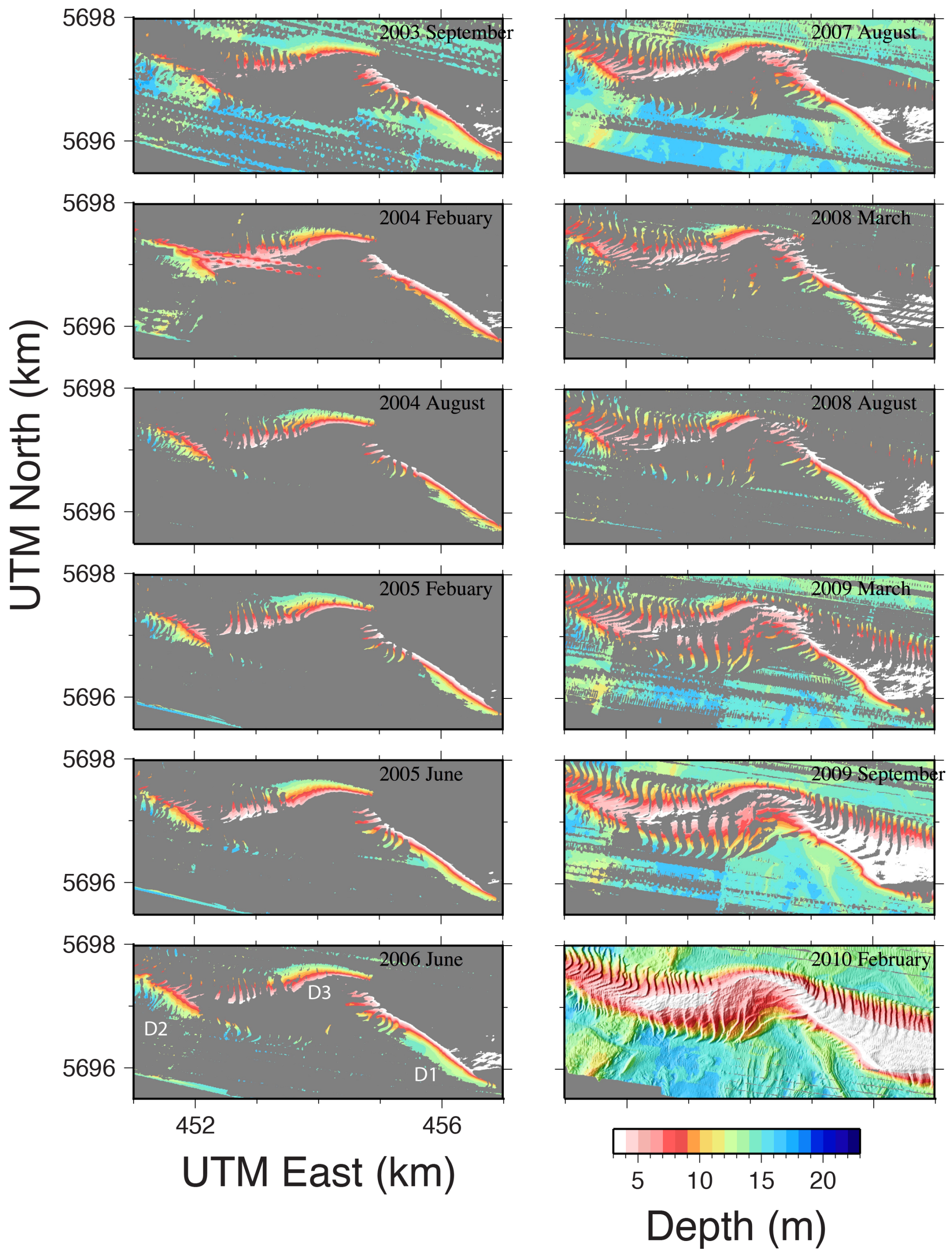

Figure 9. Stratigraphic surfaces predicted to have remained by February 2010, if all seabed surfaces were preserved.

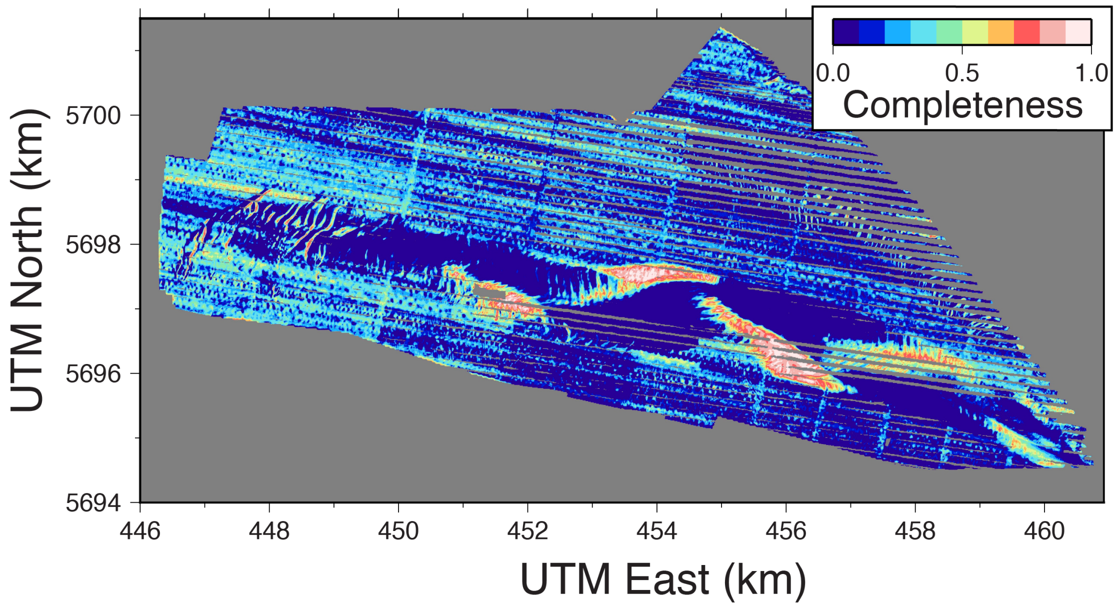

Figure 10. Stratigraphic completeness for the interval February 2003 to February 2010. Completeness is the ratio of net deposited thickness over the interval to the sum of deposited thicknesses for each interval.

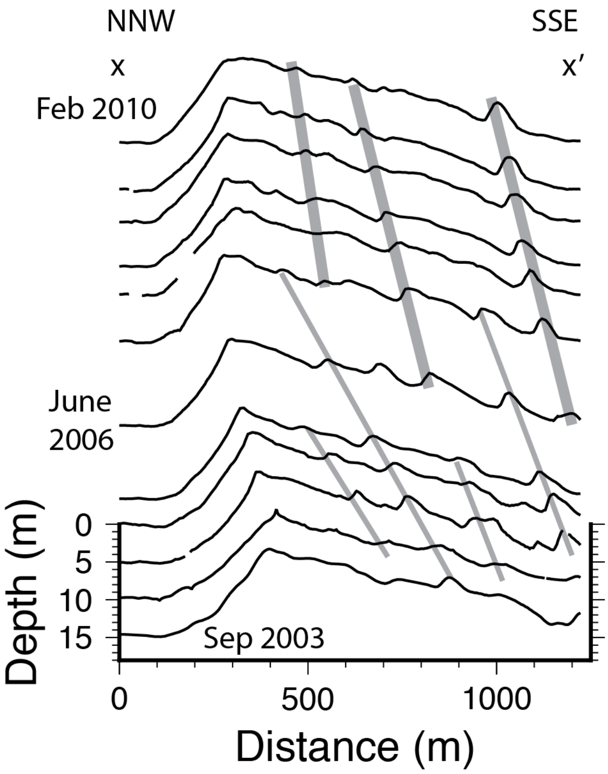

Figure 11. Bathymetry profiles crossing the swatchway along line x-x' located in Figure 2. Profiles have the same scale but are separated vertically in proportion to the time of survey since the first survey (vertical scale relates to the September 2003 profile). Bold grey bars highlight a series of migrating dunes with crestlines oriented perpendicular to the profile. Lighter grey bars highlight dunes that are oriented more obliquely to the profile, which therefore appear to have migrated more rapidly (an artefact of profile orientation).

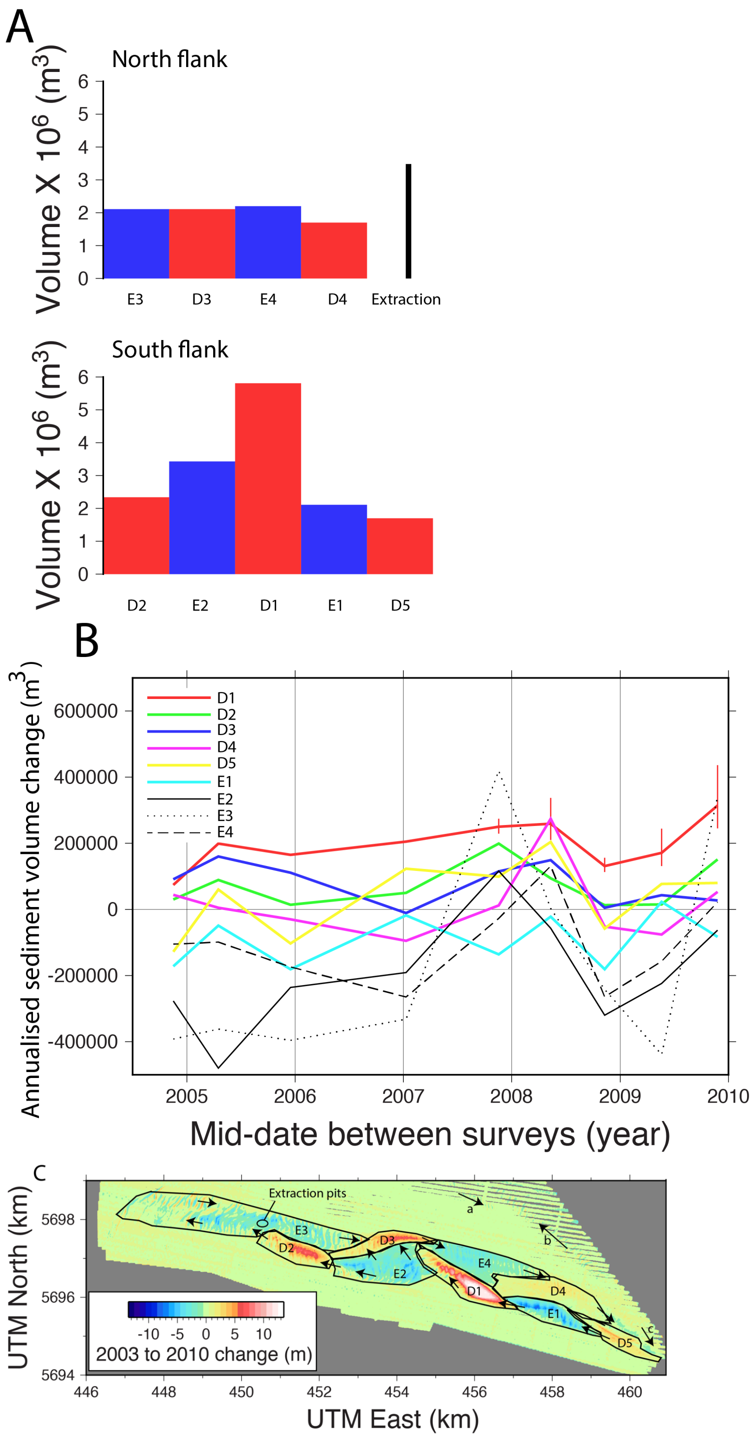

Figure 12. (a) Magnitudes of eroded and deposited volumes in each of the polygons marked in (c). Value for commercial extraction is based on the 20-year average tonnage reported by HR Wallingford (2016) scaled to 7 years and assumes a dry sand density of 1600 kg m^{-3}. Extraction occurred on West Nash, potentially affecting E3. (b) Time-series of annualised volume changes within the polygons (data before 2005 excluded due to greater noise from tidal correction errors). Uncertainty bars on D1 represent the maximum effect of uncertainty of survey dates. (c) Erosional and depositional polygons marked on a map of elevation changes from 2003 to February 2010, as Figure 5. Arrows schematically illustrate the sand movement directions suggested by bedform migrations in Figure A1a.

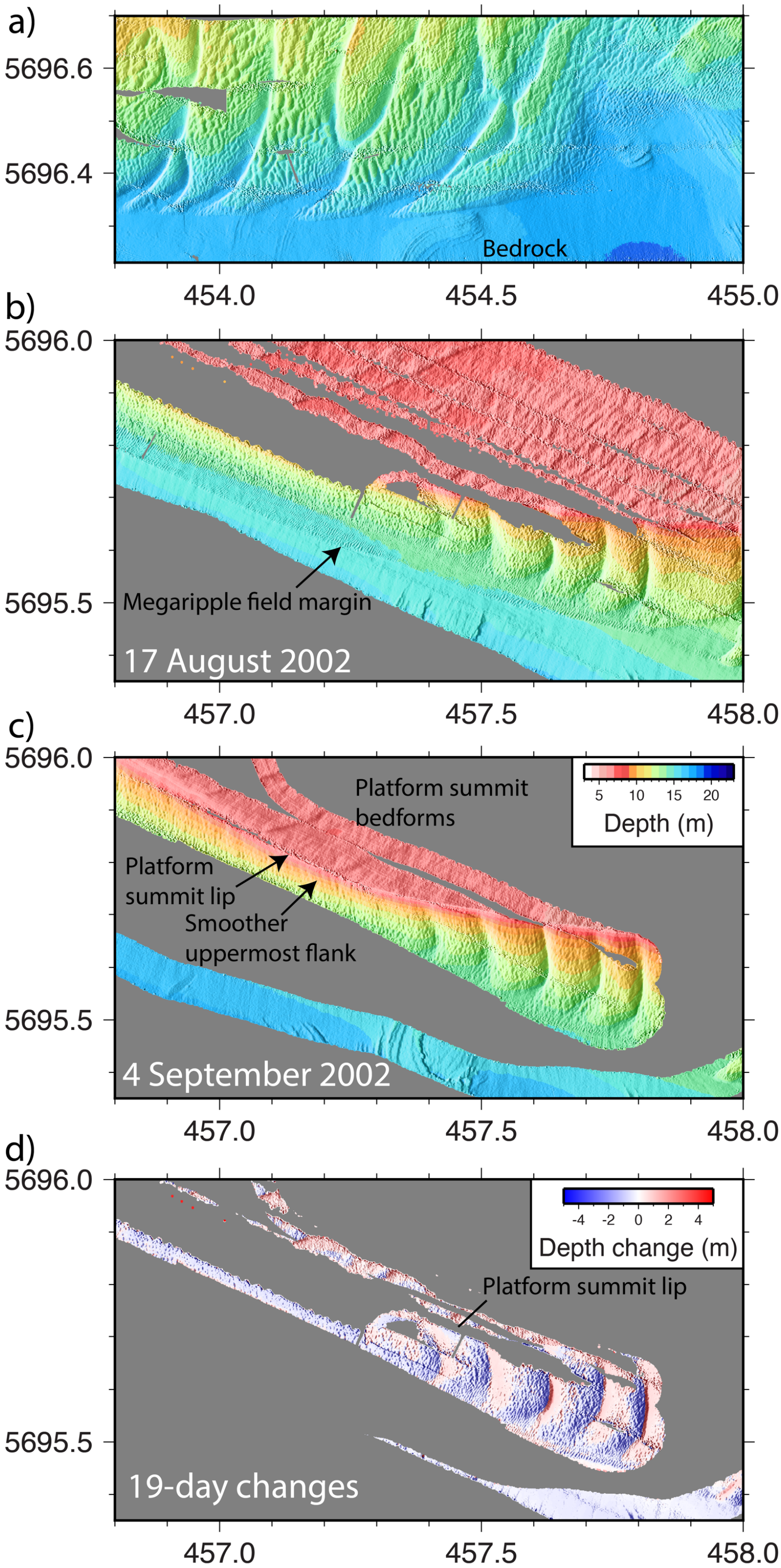

Figure 13. Enlargements of the 1-m resolution 2002 multibeam data. (a) Area eroding in west side of swatchway. (b) and (c): Southwesterly flank and summit of East Nash surveyed on the two dates shown. (d) Change from (b) to (c).

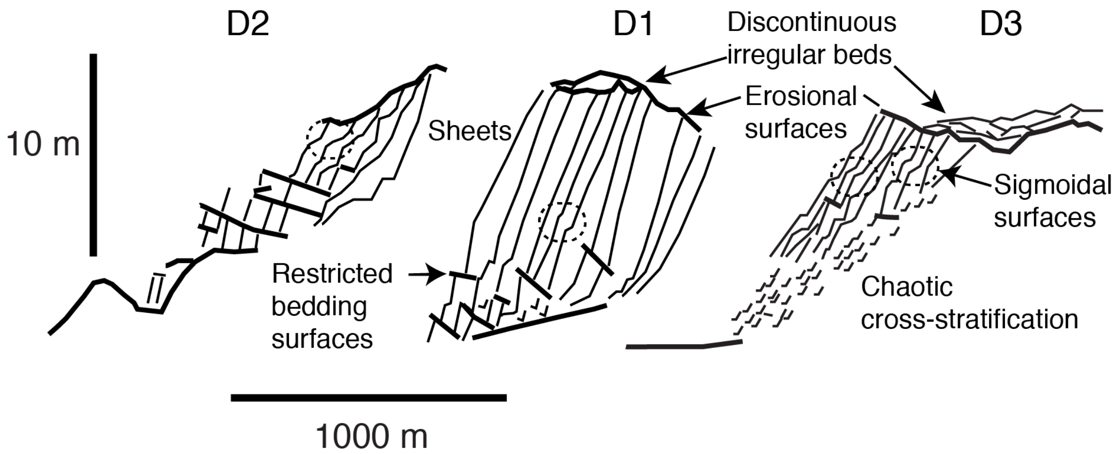

Figure 14. Schematic stratigraphy derived from Figure 6. Bold lines represent bedding and erosional surfaces. Finer lines represent cross-stratification.

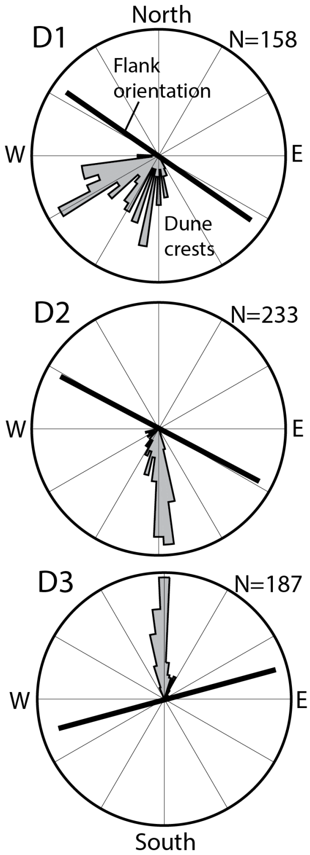

Figure 15. Directional histograms (grey) of crestlines of all lower-flank dunes lying within depositional areas D1-D3. To construct these, the orientations of the crestlines of all dunes entering each of the D1-D3 polygons (Figure 12c) in all 2002-2010 multibeam surveys were measured. Those orientations were binned at 5˚ intervals to produce these histograms. Bold bars represent the strikes of the upper flanks within these depositional areas (i.e., the orientations of the apparent clinoforms) measured from the March 2008 multibeam data. If crestlines are perpendicular to the residual currents and as we define accretion as perpendicular to the strike of the flank, the angle between these two measures also represents the direction of accretion relative to the currents.

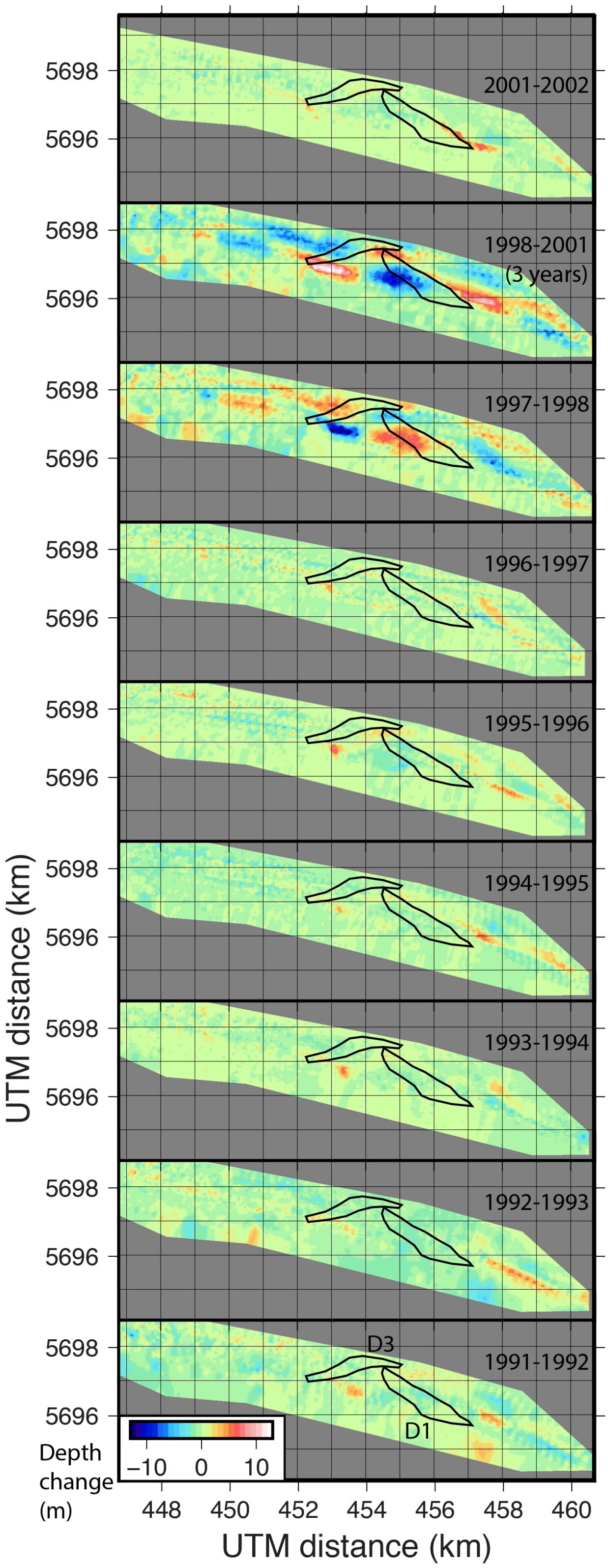

Figure 16. Bathymetric changes of Nash Sands derived from single-beam soundings 1991-2002 collected almost annually (Lewis et al., 2015). The polygons D1 and D3 from Figure 12c are shown to help comparison with the multibeam-derived maps. Note panel for 1998-2001 represents three years of change (survey data for 1999 and 2000 were not available to us).

Electronic supplement

Figure A1. Animations of the multibeam data in map form. To view these figures, set mode in PDF viewer to show one page at a time if necessary and step through each timestep in turn using the viewer forward button. (a) Multibeam data overlain with the profiles as Figure 6. (b) Enlargement of multibeam data within area D1 showing lateral accretion and migrating dunes in lower flank of the bank. Contours are every 1 m. Data for August 2002 were gridded at 1 m resolution and hence show megaripples not visible in other panels. For March 2008 onwards, red asterisks locate a trough between two closely spaced dunes that are clearly observable in a series of surveys. Black asterisks are placed in a trough along line S3. Although the dunes there are less characteristic, this trough maintains a common distance to the trough marked by the red asterisk and demonstrates climb occurring along profile S3. (c) Enlargement of multibeam data within area D2. (d) Enlargement of multibeam data within area D3. (e) Bathymetric time-series derived from the 1992-2002 single-beam data of Lewis et al. (2015) and the 2003-2010 multibeam data. Contours are every 5 m, with 10 m depth in bold. Depth colour scale as Figure A1a.

Figures A2 to A8 are animations in profile form, in which previous seabed surfaces are truncated by subsequent surfaces if deeper. To view these figures, set mode in PDF viewer to show one page at a time and step through each timestep in turn using the viewer forward button. Profiles are located in Figure 2 (Figures A2, A3, A4, A5, A6, A7, A8 correspond to E, N1, N2, S1, S2, S3, S4).